UPPSALA
UNIVERSITET

Effect of the host cell-growth rate on the invasion and infection efficacy of *T. cruzi* trypomastigotes, and the potential cell-to-cell transfer of this parasite

Elisa Escabia Herrando

Master's degree Project in Infection Biology, 45 credits.
2021-2022
Department: Molecular Biomedicine, CINVESTAV, Mexico
Supervisor: Dr. Rebecca Manning Cela

Abstract

Recent studies proposed that mammalian cell lines with slower growth rates were infected more efficiently by *Trypanosoma cruzi,* and that cell-to-cell transmission could be occurring during infection. This open the question of whether host cell-growth rate is a cellular characteristic influencing *Trypanosoma cruzi* invasion and infection. To prove if this was the case, the cell growth-rate was inhibited by starvation, reducing the foetal bovine serum concentration in the medium, and using a cell-cycle arresting drug, Baicalein. Then the percentage of infected cells of the control and the growth-modified group was measured via epifluorescence microscopy. The results did not show a strong evidence of negative correlation between the cell-growth rate and infection efficacy.

To assess if cell-to-cell infection was occurring, the percentage of infected cells in contact with other infected cells was measured. This value was compared to the stochastic probability of this event happening. The results showed that the random probability of an infected cell being next to another infected cell was much lower than the percentage obtained from the empirical data. This suggests that cell-clusters found in infections are not a random event and that the dominant mechanism of infection is a short-range one: either by cell-to-cell infection, or by the proliferation of already infected cells. To support cell-to-cell transmission, parasites potentially passing from one cell to another were inspected through confocal microscopy and actin-rich regions were found at the parasite location. To determine whether actin played a role in this event, cells with a mutation in the actin gene were infected and compared to the mock group. The results showed that the percentage of infected cells in contact with other infected cells was lower for the mutant cells, suggesting that actin could play a key role in this event.

Key words

Trypanosoma cruzi, infection kinetics, cell-to-cell infection, cell-growth rate.

Popular Scientific Summary

In this project we studied an intracellular parasite called *Trypanosoma cruzi*, a dangerous pathogen that causes Chagas Disease to around 6-8 million people worldwide. Even though many people are infected, it does not get enough attention because it mainly affects people under poverty conditions, hence its nomination of Neglected Tropical Disease by the World Health Organization (WHO). As consequence, the development of new diagnosis and treatment methods are not a priority. This parasite is mainly transmitted by kissing bugs, also known as triatomines. These insects infect people in Latin America, usually in rural areas.

When kissing bugs feed on a person, usually while this one sleeps, they take such a big bloodmeal that they need to defecate during or just after feeding. The feces will be next to the bite and when the person awakes and scratches the bite, their hand will get contaminated with the feces, which can contain the infective form of the parasite. If the person then touches the biting site, the eyes, or mouth, the parasites will be able to enter the body. Once the parasites are in the bloodstream, they can infect nearly all cells. Once inside the cells, they multiply and exit the cell to infect more cells. Another way to get infected is from mother to child during pregnancy or birth, which is the most common transmission in countries where the insect vectors are not found. The parasite can also be transmitted through blood transfusion, organ donation, or by ingestion, but it is less likely. The disease is divided into two phases: the acute and the chronic phase. The acute phase is the first one and lasts around 4 weeks. During that time, many parasites are found in the bloodstream and the person might have some general symptoms, such as fever or fatigue. This period is the best one to get diagnosed and treated, but in most cases, people don't realise they are infected and don't seek medical care. If this happens, the person will most likely enter the chronic phase. In this phase the number of parasites in the bloodstream is very low and therefore the detection of the parasites by diagnostic methods is extremely difficult. Normally, people don't have any noticeable symptoms during the first years of the chronic phase. However, the parasites are damaging the tissue of some organs without the patient knowing. The organs that will be affected depend on the strain of the parasite, which is also related to the area where people get infected. After some years, around 30% of the infected people will develop cardiomyopathy or megasyndormes, such as enlarged esophagus or colon. The most commonly infected organ is the heart, which leads to incapacity or death in many individuals. Even though a lot of people suffer from this disease, only two drugs are available, and they are not very effective after the first months of infection, in addition of being quite toxic for humans.

There is the need to find out why the parasite infects some cells more efficiently than others, such as the cells in the heart. If these characteristics were found, drugs targeting those mechanisms could be developed. We knew from previous studies that the efficacy of cell-infection in four different types of cells was higher for those that grew slower. We didn't have a clue if this was coincidence or significant, so we decided to test it. To do so, we used two cell lines and reduced their cell growth by either starving them or by using a cell-growth inhibitory drug. Then we infected them and compared the percentage of infected cells with the non-treated cells. We didn't find enough difference between the groups to say that cell-growth rate affects the infection efficacy.

Another important thing we wanted to check was if the parasites could pass from one cell to another. If this happened, it would be a very important finding since it would allow them to infect new cells without being exposed to the environment outside the cell, escaping the immune system. What we did was to fix and stain the infected cells at different times. In other words, the cells and parasites were kind of petrified and marked with different colours so we could see what they were doing at that exact time. We inspected them very carefully looking for parasites that could be moving from cell-to-cell, and we found some cases very suggestive. We also found that infected cells were forming clusters. That is to say, infected cells were very likely to be found in contact with other infected cells. We calculated how likely this was if the clusters were formed randomly, and the statistical probability was way lower. Meaning that the clusters were not formed randomly, and that cell-to-cell transmission could be a cause.

To sum up, Chagas disease is a very important health problem and there is the need to know more on the pathogenesis, so new drug targets can be found. We studied if cell-growth rate had an influence in the infection efficacy, and we didn’t find any. Also, we investigated if parasites could move from cell-to-cell and found out that it is a very likely possibility. However, more studies are needed it to confirm it, such as a live time-lapse.

Table of contents

Introduction

Chagas disease, also known as American trypanosomiasis, is a zoonosis caused by the protozoan parasite *Trypanosoma cruzi*[1]. It is mainly transmitted by hematophagous insects belonging to the subfamily Triatominae, commonly known as kissing bugs[1] (Figure 1). The disease was described for the first time over a century ago by the physician Carlos Chagas, who characterized the etiological agent, the clinical manifestations, and the insect vector [2]. Chagas disease is endemic from 21 Latin American countries and it is one of its leading public health problems, regarded by the WHO as one of the twenty Neglected Tropical Diseases[3,4]. In recent years, Chagas disease has become a global health threat due to the large-scale migration from endemic countries to Europe, North America, Japan, and Australia[5]. It is estimated that 6-8 million people are infected worldwide and 65-100 million people are at risk of infection [3,4,6]. It annually causes 10000-15000 deaths and a loss of 0.65-0.8 million disability-adjusted life years (DALYs) [6–8]. As a consequence, the yearly global economic burden of Chagas disease is estimated to be 752000 working days lost because of premature deaths[9], US$7.2 billion per year lost in productivity[8], and US$627 million per year destined to healthcare costs[8]. These costs are similar or exceed those from other prominent infectious diseases, such as rotavirus (US$7.2 billion vs US$2 billion)[10], emphasizing the need for more attention and efforts concerning the control of Chagas disease.

Trypanosoma cruzi is predominantly transmitted via contaminated feces from an infected triatomine, either via the introduction of the faeces into the biting site or a mucosal membrane[3]. The transmission cycle can be sylvatic, when triatomine insects live in the wild and feed on feral mammals that act as reservoirs, such as rodents or opossums, or domestic if triatomine insects are go inside houses and feed on humans and pets[11]. The domestic cycle is the most relevant one for human infection, but the sylvatic cycle plays a major role in being the source of infected triatomines[11]. In domestic environments, triatomines usually hide during the day in the cracks of precariously constructed homes, such as abode houses, and during the night they blood-feed on vertebrate hosts, including humans [12,13]. They bite exposed areas, such as the face or lips, hence its common name of kissing bug. While biting, the insect secretes apyrase, a protein that dephosphorylates AMP generating free adenosine with anaesthetic activity[14]. As a consequence, the human being bitten does not feel pain, allowing the insect to complete its blood meal, which usually requires 20-40min[15]. Blood meal size varies between species and life stages, usually being 2-3 times the insect body weight[15–17]. Due to the large blood intake, triatomines defecate during or just after the meal[18–21]. Unlike other vector-borne diseases, *T. cruzi* is not passed through the saliva, but the infective parasites are found in the faeces. When the aesthetic effect passes and the host awakes, they scratch themselves facilitating the entrance of the parasites at the biting site or into a mucosal membrane, such as eyes or mouth. Triatomine insects capable to transmit the disease to humans are only found in the Americas, specifically in rural areas where poverty prevails[1]. This transmission pathway is the connection between the disease and the social and economic aspects of the populations at risk[1,4]. Congenital transmission also occurs during pregnancy or childbirth, being the main infection route in non-endemic countries [3]. It can also be transmitted orally by the consumption of contaminated water or food, causing localized outbreaks[3]. In addition, infected donors can also transmit the parasite through blood transfusion and organ transplantation[3]. Vectorial and congenital transmissions are the most common pathways, accounting for 70% and 26% of the cases, respectively [22].

The clinical course of infection usually consists of an acute and a chronic phase. The acute phase generally lasts 4-8 weeks and it presents the highest parasitemia[23]. Most acute infections are asymptomatic or present unspecific symptoms, such as fever or malaise[24–27]. Consequently, only 1-2% of cases in this phase are diagnosed[26]*. The two characteristic manifestations are the Romaña sign, a unilateral palpebral oedema when the conjunctiva is the entry point, and the Chagoma, a prominent inflammation at the inoculation site[23]. Severe acute disease is usually associated with orally transmitted infections and presents a high mortality rate because of myocarditis[23,27,28]. Acute infection normally resolves spontaneously and, mostly if not treated, the patient then enters the chronic phase[23]. Parasitaemia during the chronic phase is very low and most of the cases do not present symptoms or they are very mild, which is known as the indeterminate form of infection. However, lack of evident symptoms does not mean the absence of damage, since it has been found that patients in the chronic indeterminate phase can present fibrosis in the myocardial tissue[29]. After 10-30 years, around 30% of all chronically infected patients will develop inflammatory cardiomyopathy and 5-10%, digestive disorders or megaviscera[30–32]. Sudden death, refractory heart failure, and thromboembolism are the main death causes of Chagas heart disease (CHD)[33]. Gastrointestinal syndromes are more common in the Southern Cone of South America and go from motility disorders to severe megaoesophagus or megacolon[33]. In all cases, organ damage is caused by the presence of the parasite and the acute inflammation that it triggers[33,34]. In addition, autoimmunity has also been found in cases where *T. cruzi* antigens cross-react with autoantigens[34]. Diagnosis of acute infections is done by direct visualization of trypomastigotes in blood or by PCR, and for the chronic phase, it relies on serological testing due to the low parasitemia[35,36]. There are only two available drugs to treat Chagas disease: benznidazole and nifurtimox[37]. However, it is necessary to identify new effective alternatives since both of the existing drugs only present high efficiency during the acute phase, have strong toxicity, parasite resistance has developed and they are not commercially available[37].

T. cruzi exhibits a digenetic life cycle, alternating between triatomine vectors and mammalian hosts[1]. It goes through four developmental stages: epimastigote, amastigote, and trypomastigote (metacyclic and bloodstream). Epimastigotes proliferate in the insect midgut and differentiate into metacyclic trypomastigotes, the non-replicative form that infects the mammal host through skin wounds or mucosal membranes[1,38]. Once they invade the mammalian host cells, trypomastigotes reside in a vesicle called the parasitophorous vacuole, from which they escape to the cytoplasm and differentiate into amastigotes, the second replicative stage[38,39]. After replication, amastigotes become trypomastigotes that are released into the bloodstream, enabling infection of other cells or triatomine insects biting the infected host[38]. All the developmental stages are flagellated, but only epimastigotes and trypomastigotes have a flagellum long enough to confer motility[40]. An illustration summarizing *T. cruzi* transmission cycle is found in Figure 2.

Figure 1: Image of a male adult *Triatoma barberi* taken with a stereomicroscope.

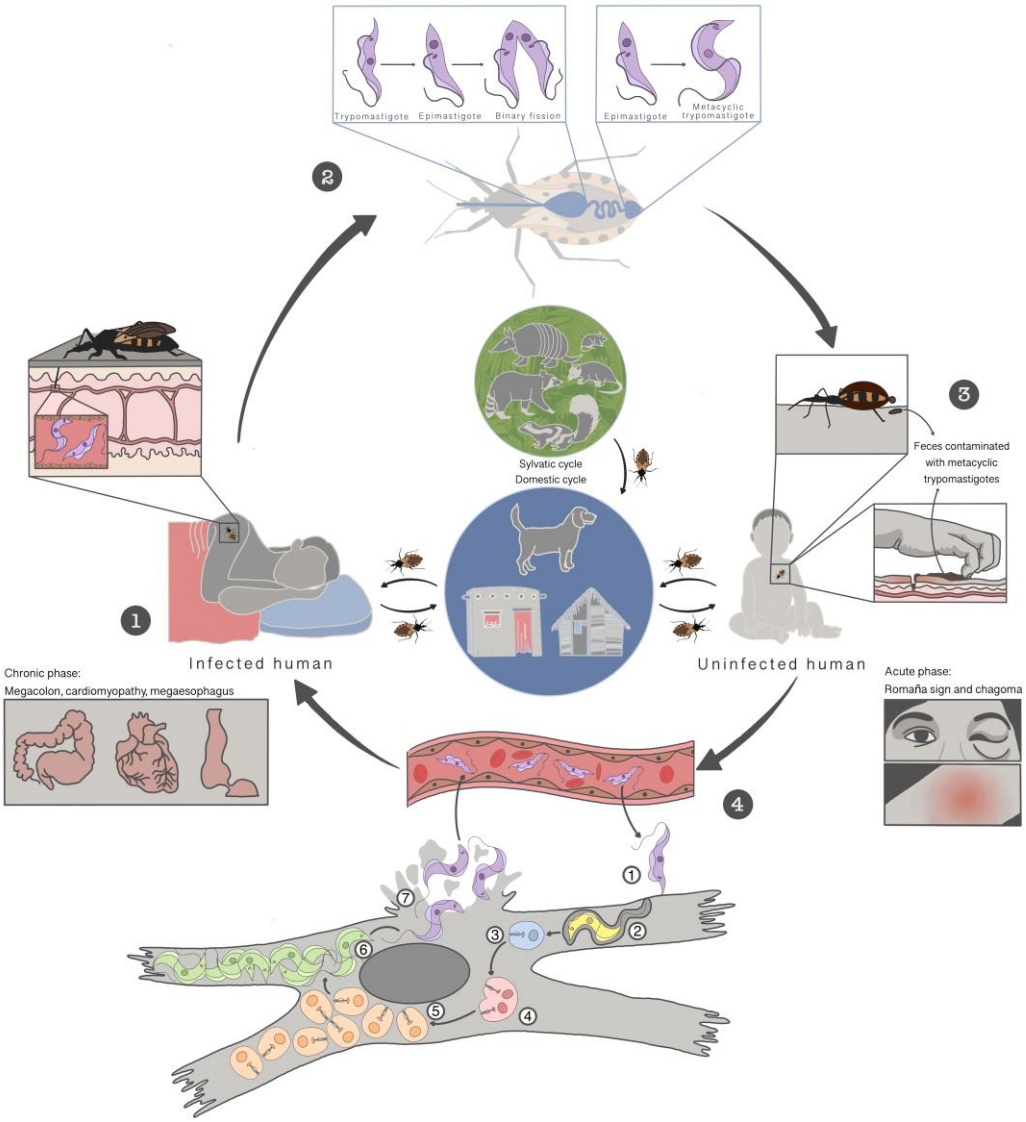

Figure 2: *T. cruzi* transmission cycle. 1) An uninfected triatomine takes a bloodmeal from an infected host, ingesting blood-trypomastigotes. 2) The trypomastigotes in the midgut of the triatomine differentiate to epimastigotes and multiply by binary fission. Epimastigotes migrate to the hindgut, where they differentiate into metacyclic trypomastigotes. 3) An infected triatomine feeds on an uninfected human and defecates close to the biting point. The human introduces the feces with infective metacyclic trypomastigotes into the biting site or a mucosal membrane, most likely because of scratching the bite. 4) Trypomastigotes swim in the bloodstream and infect nucleated cells. 1.1) The trypomastigote adheres to the cell membrane either by the anterior or the posterior end. 1.2) Through redundant pathways, the parasite enters the cell inside a parasitophorous vacuole. 1.3) Following an unknown pathway, the parasite escapes the parasitophorous vacuole either just before or after differentiating to an amastigote. 1.4 and 1.5) Amastigotes multiply by binary fission, occupying most of the cell's volume. 1.6) Amastigotes differentiate to trypomastigotes. 1.6) Trypomastigotes exit the cell before and after cell lysis. Liberated trypomastigotes will be found in the bloodstream and can either infect other cells or infect triatomines feeding on the infected host. The characteristic signs from the acute and the chronic phase are also illustrated: the Romaña sign and the inoculation Chagoma; and the megacolon, megaoesophagus, and Chagasic heart, respectively. The green cercle found in the centre of the illustration represents the sylvatic cycle, containing the most common reservoirs of the parasite: raccoon, opossum, field mouse, anteater… The sylvatic cycle is a very important source of infected triatomines, which can be introduced to the domestic cycle (blue circle). The domestic cycle is normally characterized by the presence of domestic animals, such as dogs, cats, pigs, hens, etc., and poorly constructed houses. The domestic cycle is the principal origin of human infections, and it links poverty to the disease. Illustration made on iPad with Apple Pencil and the Procreate App.

Trypanosoma cruzi belongs to the family of trypanosomatidae in the order Kinetoplastida. The genus *Trypanosoma* contains about 20 species, but only *T. brucei* and *T. cruzi* cause disease in humans[41]. *T. cruzi* is a heterogeneous species with a high genetic and phenotypic diversity, which corresponds to biological, pathological, and clinical characteristics[42]. In 2009, the parasite was classified into six discrete typing units (DTUs). Currently, seven DTUs are accepted, named TcI to TcVI and the recently added TcBat[43]. There is no consensus on the origin and evolutionary relationships between DTUs, but there are two supported models: the ”Two-hybridization”[44] and the ”Three ancestors”[45] (Figure 3). In both cases, two hybridization events occured[44–46]. In the model proposed by Westenberger et al. (2005), the ”Two-hybridization” model, TcI and TcII were the oldest DTUs, and their hybridization lead to the formation of TcIV and TcIII[44]. A second hybridization between TcIII and TcII resulted in the appearance of TcV and TcVI[44]. On the other hand, in the Three ancestors” model, Freitas et al. (2006) proposed TcI, TcII, and TcII as the original ancestors, and that two different hybridizations between TcII and TcIII produced TcV and TcVI[45]. TcI has the widest distribution and it is the most frequently found in sylvatic cycles, although it is also sampled in domestic habitats and it is the main DTU responsible for infections in the north of the Amazon basin[27,43]. Tc II, V, and VI are typical of domestic cycles and are dominant in the southern cone[27,43]. TcII and IV are mainly found in sylvatic cycles in the rainforest and are not known to have an important role in human transmission[27,43]. TcBat is mainly found in bats, even though it has also been identified in humans[43].

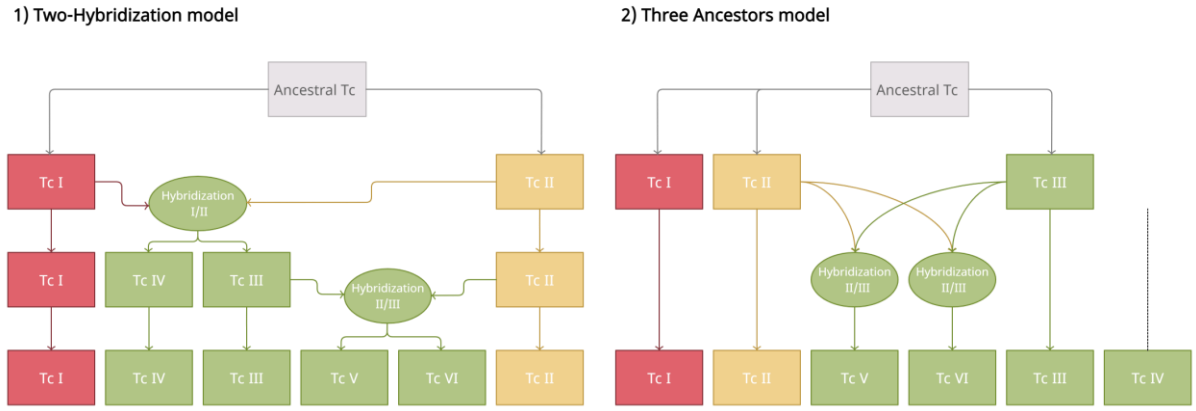

Figure 3: Evolutionary trees based on the Two-hybridization and the Three ancestors models. The rectangles correspond to DTUs and the ovals to hybridization events. The mitochondrial clades are colour-coded in red (clade A), green (clade B), and yellow (clade C). The illustration was done based on the review published by Zingales et al. (2012).

The parasite *T. cruzi* invades mammalian cells following several pathways. Commonly, it consists of four major steps: host cell recognition and adhesion, parasite internalization, parasitophorous vacuole formation and maturation, and its release into the cytosol[39]. There are three main mechanisms for internalization: recruitment of lysosomes, endocytosis, and autophagy. Tardieux et al. (1992), revealed for the first time an actin-independent mechanism for cell invasion that involved the recruitment of lysosomes for fusion at the site of internalization[47]. During trypomastigote cell-invasion, a directional microtubule/kinesin-mediated migration of lysosomes to the entry site occurs[48]. This lysosome-mediated invasion is triggered by Ca^{2+} release from cellular compartments enhanced by an increase of cAMP levels[39]. The endocytic pathway includes different processes, such as phagocytosis, clathrin-mediated endocytosis, and macropinocytosis[39]. Phagocytosis dependent on PI3-kinases accounts for over 50% of trypomastigotes invasion[39,49]. Extracellular amastigotes also follow a phagocytosis-like pathway to enter the cell[50,51]. Clathrin was observed around the parasite at the cell entry point and, when clathrin-coated vesicle formation was inhibited, trypomastigote and amastigote invasion decreased[52]. Micropinocytosis, an actin-mediated mechanism to endocytose large amounts of solutes, is also used by *T. cruzi* to enter the host cell[53]. Proteins participating in macropinosome formation were visualized at the parasite entry site and, when micropinocytosis' inhibitors were used, invasion was blocked[53]. In addition, it has also been demonstrated that *T. cruzi* can modulate cell autophagy to invade the cell[54,55]. Autophagy is a cellular self-digestion process involving the lysosomal machinery[55]. The interruption of mammalian autophagy reduces the parasite infectivity and autophagic proteins were found in the parasitophorous vacuole[55,56]. Also, the induction of mammalian autophagy by starvation stress increased infectivity by enhancing the number of available lysosomal compartments[55]. Recent studies also suggested the possibility of cell-to-cell infection[57].

Arias-del-Angel et al. (2020) proposed distinct mathematical models to fit the infection kinetics by trypomastigotes in various mammalian cell lines[57]. The simplest model, which only considered cell-parasite infection and replication of non-infected cells, was not able to reproduce the experimental outcome[57]. A second model, which also included cell-to-cell infection, was capable to replicate the experimental results[57]. The reasoning behind this difference is that during the infection experiment, parasites were removed from the medium every second day. As a consequence, if cell-to-cell infection was not occurring, infection should stop until new parasites were released. However, this was not observed in the experimental data[57]. Cell-to-cell infection has never been recorded for *T. cruzi*, but it has been demonstrated for other cytosolic pathogens. Bacterial cell-to-cell spread has been observed in many species[58]. For instance, *Shigella, Rickettsia,* and *Listeria* manipulate host proteins to form actin tails that propel them into the plasma membrane and create protrusions that introduce them to the neighbouring cell[58,59]. A similar mechanism is used by *Mycobacterium tuberculosis* and *Mycobacterium marinum*, which are ejected from the donor cell through an actin structure named ejectosome[60]. This transmission pathway was then found to be related to autophagy since a membranous cup formed by the canonical autophagic pathway was located at the ejection point[61]. If autophagy was inhibited, *Mycobacterium* cell-to-cell transmission reduced significantly and cell membrane stability was compromised leading to cell death during ejection[61]. *Burkholderia*, in addition to forming actin tails, can induce the host cell-cell fusion forming a multinucleated giant cell[62,63]. Yeast cell-to-cell spread was documented for the first time in 2007 by two independent studies published simultaneously[64,65]. Live imaging of the interaction between *Cryptococcus neoformans* and macrophages showed that the yeast escapes the intracellular limits of macrophages in an actin-dependent process, leading to the infection

of neighbouring cells[64]. Another pathogen closely related to *T. cruzi* that also exhibits cell-to-cell transmission is *Leishmania*[66,67]. Using multidimensional live imaging, Real et al. (2014) observed that *L. amazonensis* amastigotes were extruded from apoptotic macrophages and selectively internalized by healthy recipient macrophages[67]. This was further validated in *L. aethiopica* and *L. mexicana*, confirming that amastigotes protrude from zeiotic structures rich in lysosomal-associated membrane protein 1 (LAMP-1)[66,68]. Another protist that can spread to adjacent cells is *Toxoplasma gondii*[69]. The sporozoites contained in the parasitophorous vacuole posteriorly release proteins that form a membranous tail, propelling them towards the cell membrane[69]. Followed by the formation of finger-like protrusions, the parasites can form a cell-to-cell passage and enter the adjacent cell, probably maintaining the parasitophorous vacuole membrane[69]. All these mechanisms of cell-to-cell infection serve to escape the immune system and could be involved in the establishment of persistent infections.

In this study, the potential cell-to-cell transfer of *T. cruzi* amastigotes and trypomastigotes was evaluated by calculating the probability of an infected cell to be in direct contact with another infected cell. The results were validated with a mathematical model that concludes whether the found probability is caused or not by a random event. In addition, cells infected with fluorescent parasites were fixed and stained to be inspected by confocal microscopy, expecting to find a parasite passing from one cell to another. Since many intracellular pathogens use actin to be transferred to a neighbouring cell, it is speculated that it could also play a role in the case of *T. cruzi.* To test whether this is the case, the percentage of infected cells in contact with other infected cells was compared between the control group and cells transfected with a mutation in the actin gene, which diminishes actin polymerization.

Despite the ability of *T. cruzi* to invade any nucleated host cell type, the disease is characterized by the infection of specific tissues, such as cardiac and skeletal muscle[33,70]. It is not known, however, why do parasites invade some cell types more efficiently than others. Previous studies found that *T. cruzi* motility was influenced by the presence of in-vitro-cultured mammalian cell lines[40]. Trypomasgotes increased their mean speed, dispersed less, and preferred to be close to the cells. These changes were also dependent on the cell type, suggesting that they can sense the presence of specific cell lines[40]. It was further investigated if these changes influenced the invasion efficiency, and the results suggested a possible correlation between the extent of motility changes and invasion efficiency[40]. Interestingly, this study also found a negative correlation between the susceptible cell growth rate and the percentage of infected cells and the average parasite count per cell[57]. In other words, cell lines that grow at a slower pace were infected more and had a higher number of parasites per cell. Suggesting that cell-growth rate could be one of the host cell characteristics that enhances *T. cruzi* invasion and infection efficiency. To validate this hypothesis, infection kinetics experiments modifying the cell growth rate of specific cell lines were performed.

To summarize, during the over 100 years since Chagas disease discovery in Latin America, it has become a worldwide problem and it is still missing a cure[4,33,35]. The mechanisms behind tissue tropism during *T. cruzi* infection remain poorly understood, although they have been linked to transmission enhancement, treatment failure, and the clinical outcome[71]. Therefore, it is of great importance to understand the cell invasion and infection processes that cause pathology and enable the establishment of the infection, including new transmission pathways such as cell-to-cell spread.

Aim

This project aimed to answer two main questions: whether host cell-growth rate influences *T. cruzi* invasion and infection, and if cell-to-cell transfer is occurring during *T. cruzi* infection.

In order to answer the first question, it was needed to find a strategy to modify the cell growth rate. The first step was to identify a technique to count cells efficiently, since the cell number was needed to find the half-maximal inhibitory concentration (IC50) of a drug arresting the cell cycle. Afterwards, an infection kinetics experiment had to be designed and performed, in which the percentage of infected cells of a control group and a group of cells with their growth rate inhibited was compared.

The second research question had the objective to design an infection assay that allowed for the visualization through microscopy of a parasite passing from one cell to another, and to suggest or prove this event via mathematical models. In addition, in case the previous experiments suggested that cell-to-cell transfer was occurring, an experiment testing the role of filamentous actin in this event would be designed and performed.

Materials and methods.

Reagents

Dulbecco' Modified Eagle's Medium (DMEM) for cell culture was prepared mixing the medium with sodium bicarbonate in distilled water and adjusting the pH to 6.8 with concentrated HCl. It was then sterilized with a vacuum filter of 0.22 microns. Complement of Foetal Bovine Serum (FBS) was heat-inactivated in an agitating water-bath at 56ºC for 30min. PBS 1x was prepared dissolving NaCl, K_2HPO_4 and KH_2PO_4 in distilled water (pH: 7.4) and autoclaving for 45min at 121ºC. The Liver Infusion Tryptose (LIT) medium was prepared mixing in distilled water NaCl, KCl, Na_2HPO_4, glucose, liver infusion and tryptose. Hemine was prepared to a final concentration of 5mg/ml by dissolving hemine in NaOH 0.1M and sterilizing by filtration. Baicalein was dissolved in DMSO and PBS 1x to a final concentration of 4mM, with a DMSO concentration of 2.43M. Indisulam was dissolved as well in DMSO and PBS 1x to a final concentration of 2.5mM, with a DMSO concentration of 2.47M. Both Indisulam and Baicalein were stored at -20ºC. Formaldehyde 3.7% was prepared dissolving formaldehyde 37% in PBS 1x. Hank's Balanced Salt Solution (HBSS) was prepared dissolving in distilled water: NaCl, KCl, $CaCl_2$, $MgSO_4 \cdot 7H_2O$, $MgCl_2 \cdot 6H_2O$, $NaHPO_4 \cdot 7H_2O$, KH_2PO_4, D-glucose, $NaHCO_3$. It was then autoclaved for 45min at 121ºC. DAPI (4',6-diamidino-2-phenylindole) was dissolved in MilliQ water 1:20000, and rhodamine phalloidin was dissolved in PBS 1x 1:1000. They were both prepared just before use and maintained on ice and covered with aluminium foil.

Cell cultures

The cell lines used in this study were chosen based on their susceptibility to *T. cruzi* infection and their relation to the organs where the disease pathology occurs. The cell lines were: 3T3 NIH embryonic mouse fibroblasts (ATCC CRL-1658), 3T3 Swiss-Albino (3T3-S) embryonic mouse fibroblasts (ATCC CCL-92), and H9c2(2-1) rat myoblasts (ATCC CRL-1446). They were grown in DMEM supplemented with 10% (v/v) FBS and 0.5% (v/v) penicillin/streptomycin (100µl/ml), at a humidified atmosphere of 5% CO_2 and 37ºC. They were subcultured three times per week by trypsinisation avoiding cells to grow over 90% confluence.

Parasite cultures

The strain CL Brener was the one used in this study since it is the reference strain for the genome project, and it is well characterized. Fluorescent epimastigotes were maintained in LIT medium supplemented with 10% (v/v) FBS, 0.5% (v/v) penicillin/streptomycin (100µl/ml), and 0.5% (v/v) hemine (5 mg/ml), at 28ºC. The stable transfected epimastigoes were obtained from previous work in the laboratory[72].

Cell-culture-derived trypomastigotes

Cell-culture-derived trypomastigotes (CCDT) were obtained from the supernatant of 3T3-NIH primary infections. Primary infections were conducted on 3T3-NIH monolayers at 50% confluence. T-25 or T-75 flasks with filter lids were infected with $1x10^7$ or $3x10^7$epimastigotes at mid-log-phase growth, respectively, in DMEM supplemented with 2% (v/v) FBS and 0.5% (v/v) penicillin/streptomycin (100µl/ml). Before infecting, epimastigotes were washed carefully by centrifugation with DMEM to remove all the hemine, which it is added to the supplemented LIT medium where epimastigotes are grown. The lack of hemine and FBS enhances epimastigote differentiation to trypomastigote. Every forty-eight hours, the cells were washed with DMEM to remove free-swimming parasites and fresh DMEM with 2% FBS was added. After 5-7 days, the released trypomastigotes found in the supernatant were recovered and used immediately for secondary infections. Secondary infections were also performed in 3T3-NIH monolayers at 50% confluence with the same number of parasites. Trypomastigotes from the primary infections' supernatant were centrifuged and counted before infecting with DMEM supplemented with 2% FBS. To avoid contamination by amastigotes, only the trypomastigotes released during the first 3-4 days from secondary infections were used in the experiments described below.

Methylene blue assay

The methylene blue assay is a direct technique to count cells by staining fixed cells with methylene blue, which binds to the cellular nucleus and matrix. After washing the cells, the pH is lowered with an elution buffer to liberate the dye. Then, the optical density of the elution buffer is measured, which correlates to the cell number[73,74]. In this project, this assay was used to perform dose-response curves. First, cells were grown to the desire confluence in 96-well plates (Corning, Sigma-Aldrich, USA). The medium from the wells was removed by overturning the plate in a clean container and pressing it on absorbent paper. This was done to reduce the damage on the monolayer caused by aspiration, either from the vacuum system or the pipette, which was observed while setting the conditions of this assay. Then the cells were washed with 200µl of PBS 1x, which was removed in the same way as the medium. Subsequently, the cells were fixed and stained with 50µl of HBSS containing 0.6% (v/m) methylene blue and 3.7% (v/v) formaldehyde and incubated for one hour at 37º C and 5% CO_2. Cells were fixed and stained simultaneously to avoid unnecessary steps that could enhance their detachment. The exceeding methylene blue solution was washed by submerging the plate in distilled water six times and it was allowed to air-dry for 2 minutes. The methylene blue dye bound to the cells was eluted with 150µl of HCl 0.1M. After 30 minutes at room temperature in the dark, the HCl from the wells was homogenized by pipetting 10 times and 100µl were seeded in a 96-well reader plate. The optical density was read using a spectrophotometer with a wavelength of 562nm. A standard curve was always performed using dilution series of known cell concentrations. The linear regression equation was used to estimate the cell number if the coefficient of determination (R^2) was greater than 0.9. One of the constraints from this assay was that the cell monolayer was in some cases damaged when processing them. This was the case for the cell lines H9c2 and 3T3-NIH, causing the R^2 value to be lower than 0.7. Consequently, this assay was only used to count 3T3-S cells in the experiments below, which did have a R^2 greater than 0.9.

Curve-response assay

The IC50 from Baicalein and Indisulam, two cell-growth inhibitory drugs, was obtained using the methylene blue assay to quantify the cell number at different time points using distinct drug concentrations. In addition, the effect of FBS was also analysed following the same principle. This experiment was only performed on 3T3-S cells because 3T3-NIH and H9c2 cells could not be used in the methylene blue assay, due to their weaker adhesion.

The stock solutions of Baicalein (4mM) and Indisulam (2.5mM) were diluted in DMEM supplemented with 10% FBS to a series of concentrations based on the IC50s found in the literature. The concentrations used for Baicalein were: 80µM, 40µM, 20µM, 10µM, 5µM, 2.5µM , 1.25µM , and 0.625µM[75–77]. In the case of Indisulam, the concentrations were: 12µM, 6µM, 3µM, 1.5µM, 0.75µM, 0.375µM, 0.1875µM, and 0.094µM[78–80]. In addition to a negative control, the experiment also included a control for DMSO since it was used to prepare the stock solution, using the highest concentration in which it was found: 47.9mM.

The 3T3-S cells were plated in triplicates on 96-well cell-culture plates (Corning, Sigma-Aldrich, USA) with an initial cell number of $1x10^5$ cells per well. Five 96-well plates were seeded, one for each analysed time. In the case of Indisulam and Baicalein, they were plated with DMEM supplemented with 10% FBS and the corresponding drug concentration. For the FBS dose-response curve, the cells were plated with DMEM and the following percentage of FBS: 0, 0.5, 1, 1.5, 2, 2.5, 5, 10. An illustration of the plating is shown in Figure 4. Cells were incubated at 37ºC and 5% CO_2 for 7h to allow their attachment and then the cell growth number was measured using the methylene blue assay at 7h, 24h, 48h, 72h, 96h. Seven hours was considered the time zero and no significant growth differences were expected. Curve-response curves were plotted for each time and condition.

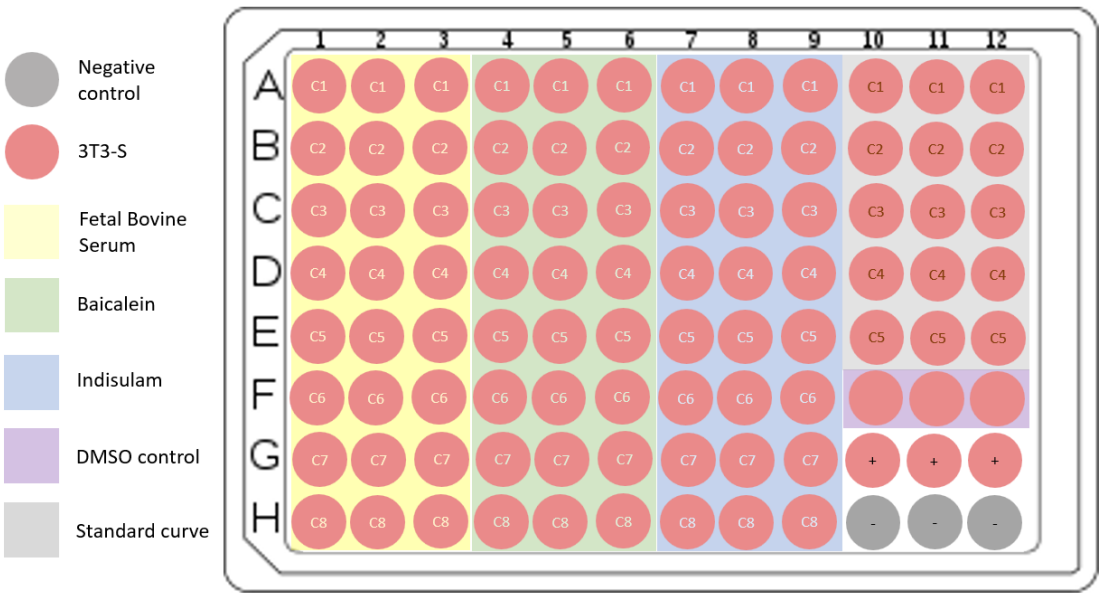

Figure 4: Plating scheme of the dose-response curves for Indisulam, Baicalein, and Foetal Bovine Serum (FBS). The red circles correspond to wells were $1x10^5$ cells were plated. Gray circles are wells where no cells were plated and only the medium was added. The wells also include a script of C1-C8, which means the drug/FBS concentration (from higher to lower). The treatment groups are classified by colours: FBS (yellow), Baicalein (green), Indisulam (blue). In addition, to the positive and negative controls, a DMSO control was included (purple - 47.9mM). A standard curve with 5 known cell concentrations was also plated (grey).

Cell-growth rate restriction assay

Based on the results from the curve-response assay, FBS reduction and the IC50 of Baicalein were used to inhibit the cell-growth rate of 3T3-S cells. In rutinary infections, cells are grown with DMEM supplemented with 10% of FBS, and during and after the infection the medium is maintained with 2% FBS. To study the effect on the cell growth of both the reduction of FBS and the IC50 of Baicalein, the following experiment was performed. The first 48h correspond to the pre-treatment of the cells, 48h would be the infection time, and the next hours are the infection.

The 3T3-S cells were plated on 96-well cell-culture plates with DMEM supplemented with 10% of FBS, either with the presence or the absence of Baicalein. After 48h, the medium was changed, as it would happen in routinary infections. In the case of the cells grown in the absence of Baicalein, the medium was changed to either DMEM supplemented with 10% (A) or 2% (B). Cells grown with Baicalein, were changed to medium with DMEM 10% + IC50 Baicalein (C), DMEM 2% + IC50 Baicalein (D), or DMEM 2% (E). A schematic illustration can be found in Figure 5.

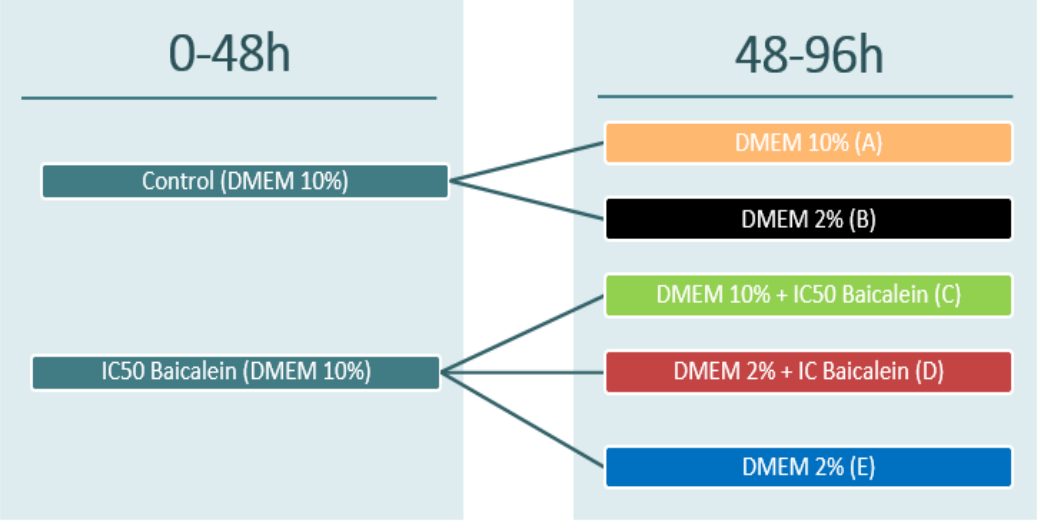

Figure 5: Schematic illustration of the treatments used for the cell-growth restriction experiment. The colour code corresponds to the one found in the results section. During the first 48h (pre-treatment), both groups were grown with DMEM supplemented with 10% FBS, but one of them was also in the presence of the IC50 of Baicalein. In the case of the cells grown in the absence of Baicalein, the medium was changed to either DMEM supplemented with 10% (A) or 2% (B). Cells grown with Baicalein, were changed the medium to DMEM 10% + IC50 Baicalein (C), DMEM 2% + IC50 Baicalein (D), or DMEM 2% (E).

The A group corresponds to the normal growth of 3T3-S cells. Group B is the situation of routinary infections. Group C only studies the effect of Baicalein on the cell growth. Group D assesses the combination of Baicalein and a reduction in the percentage FBS. Group E aimed to determine whether the pre-treatment with Baicalein was enough to inhibit the cell growth during infections.

Using the methylene blue assay, cells were quantified at 7h, 24h, 48h, 72h, and 96h. The quantification at 48h was done before the medium was changed. Then the growth curves for each treatment were compared.

Infectivity assay in cells with modified growth rate

The 3T3-S cells were treated and/or pre-treated to inhibit their growth rate and evaluate its effect on invasion and infection. An illustration summary can be found in Figure 6.

Cells were pre-treated for 48h prior to infection with either DMEM with a reduction of FBS (2% vs 10%) or with DMEM 10% with the IC50 of Baicalein. One million cells were seeded in triplicates in 60mm Petri dishes not treated for cell culture containing 3 glass coverslips (18x18mm). This was performed 7h prior to infection in order to allow for proper attachment but avoiding different cell numbers in the distinct groups at the infection time.

After seven hours the cells were seeded and the medium was changed to DMEM supplemented with 2% FBS, and with the presence or absence of Baicalein. Then, $2x10^6$ trypomastigotes transfected with the sequence coding for the Green Fluorescent Protein (GFP) were added per plate. Even though theoretically the multiplicity of infection (MOI) is 2, it is probably closer to 3 due to not all cells attaching to the glass coverslips. The interaction between cells and parasites was allowed for 2h, and then the supernatant was removed using the vacuum system. DMEM medium was added to the flask and washed twice before adding the final medium, which was DMEM supplemented with 2% of FBS, and Baicalein if necessary. One coverslip was extracted from each group and time (18h, 48h, and 96h). They were fixed with formaldehyde 3.7% and permeabilized with acetone, then they were stained with rhodamine phalloidin and DAPI.

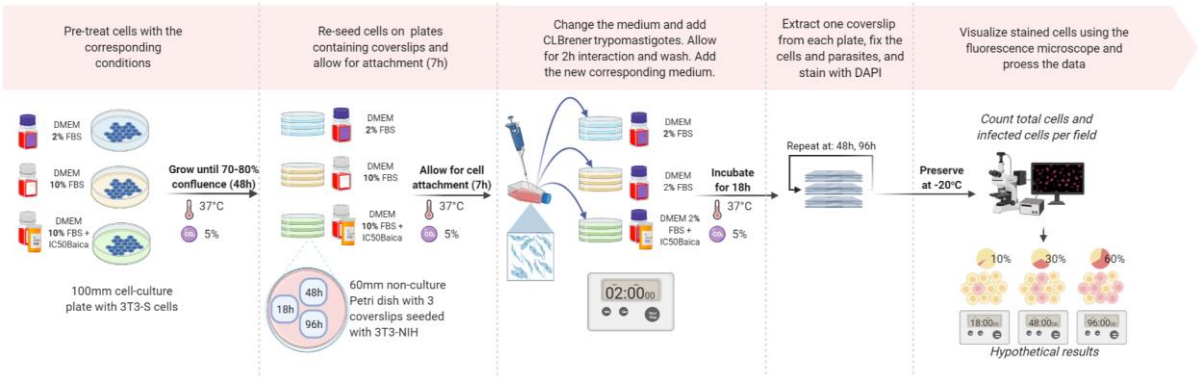

Figure 6: Graphic summary of the experiment using 3T3-S cells with modified cell growth. Designed using Biorender.com.

The stained coverslips were visualized using epifluorescence microscopy to count the total and infected cells. Cells were counted in 25 random microscope fields with an objective of 40x. A cell was considered infected if it contained at least one amastigote. The percentage of infected cells was used to assess invasion (18h) and infection (48h, 96h). In addition, the probability of an infected cell to be next to another infected cells was quantified by assessing 35 random infected cells from each coverslip. If the infected cell was in contact with one or more infected cells, it was also determined to which cell-cluster they belonged, how many parasites they contained, and the microscope filed identifier.

The results were verified repeating the experiment with the pre-treatment of FBS reduction (DMEM 2%) in 3T3-NIH cells. The exact same steps were used, including the number of cells and parasites per plate.

Coverslip processing – fixing and staining

Glass coverslips (18x18mm) were used to study the progress of infections over time. They needed to be fixed and stained with fluorescent dyes before inspecting them. To process the coverslips, 6-well plates were used. Each well to be used was filled with 2ml of PBS 1x. Then, a pair of tweezers was sterilized washing it with ethanol 70% and passing it through a flame. They were used to extract the coverslips from the infection plate and add them to the well with PBS 1x. It was very important to face the cells upwards and remember through the process their orientation. After removing the PBS 1x using the vacuum system, 1ml of formaldehyde 3.7% was added. They were incubated at room temperature for 20 min. Afterwards, the formaldehyde was aspirated, and the cells were washed twice using 2ml of PBS 1x.

Before staining with rhodamine phalloidin, cells were permeabilized by submerging the coverslips for 5min in ice-cold acetone. After that time, 300µl of phalloidin rhodamine solution (1:1000) were added on top of the coverslip. They were incubated for 20min in the dark. Then, the phalloidin rhodamine was washed by vertically submerging the coverslip in cold PBS 1x and moving 10 times from side to side. Then the coverslip was dried by standing it on paper and put again in the well. One millilitre of DAPI (1:20000) was added to the well and it was incubated in the dark for 5min. The DAPI was washed by vertically submerging the coverslip in water and moving 10 times from side to side. Then the coverslips were put on a microscope slide with 5µl of Vectashield and the cells facing down. They were allowed to air-dry for 30min before sealing them with polish. The slides were stored at -20ºC in the dark.

Effect of the IC50 of Baicalein on epimastigotes

Baicalein is a drug used to inhibit cell growth, therefore it could also affect the replicative forms of *T. cruzi* (i.e.: amastigote and epimastigote). The infectivity assay was performed using trypomastigotes, and no effect was expected on the invasion since they do not divide. However, further times of infection could be affected if the binary fission of amastigotes was inhibited. The test was done in epimastigotes instead of amastigotes because they are easier to maintain in culture. It was assumed that if Baicalein did not have an effect on epimastigotes, it would most likely not affect the division of amastigotes.

In 15ml Falcon tubes, $7.5x10^6$ epimastigotes were added in 5ml of complemented LIT medium. The treatment group also contained the IC50 of Baicalein calculated for 3T3-S cells. Both the control and the treatment group were run in triplicates. After 24h, epimastigotes were counted using the Neubauer Chamber.

Cell re-infection

Cells were infected simultaneously with trypomastigotes transfected with the sequence that encodes for GFP or the Red Fluorescent Protein (RFP). The objective was to determine whether there were cells infected with green and red parasites at the same time. If this was the case, it would suggest that parasites can reinfect an already infected cell.

In 60mm culture plates with 3 glass coverslips (18x18mm), 3T3-NIH cells were grown to 50% confluence. Then, $1.5x10^6$ CCDT expressing the gene for GFP and $1.5x10^6$ CCDT expressing the gene for RFP were added to the plate. Interaction between cells and parasites was allowed for 48h and then the coverslips were fixed and stained with DAPI and rhodamine phalloidin, following the above-mentioned procedure. The coverslips were visualized using epifluorescence microscopy, looking for cells that could be infected with parasites expressing the genes for GFP and RFP.

Laser scanning confocal microscopy

Laser scanning confocal microscopy was used to visualize cells where a parasite was suspected to be passing from one cell to another. Fixed and stained parasites and cells were scanned using a Leica TCS-SP8/DM6000 confocal microscope. The used lasers were a LASOS diode laser of 405nm, a type of OPSL laser 488nm, and a laser OPSL 552nm. The obtained file was processed using the ImarisViewer 9.9.0 software to obtain cross-section images and 3D models.

Testing the role of filamentous actin in cell-to-cell parasite transfer

Many intracellular pathogens use the host cell filamentous actin to migrate from one cell to another. Therefore, the potential role of actin in the cell transfer of *T. cruzi* parasites was evaluated.

An infectivity assay was performed using 3T3-S cells transfected with a sequence that adds a mutation in the nucleotide 174 of the gene coding for actin, obtaining a dominant negative mutant. As a consequence, the cell actin polymerization was reduced. Another group consisted of 3T3-S cells that were treated with cytochalasin D, which is a fungal toxin that causes the immediate disruption of actin filaments, inhibiting polymerization. It was added after invasion (18h) because actin-mediated pathways are known to be involved in the parasite internalization, and only cell-to-cell transfer was aimed to be affected. Cytochalasin D (2µM) was added to the plates after processing the coverslips for 18h. The drug was left for 30h before changing the medium.

Via epifluorescence microscopy, the infection percentage and the probability of an infected cell to be in contact with other infected cells were quantified. A schematic representation of the experiment can be found in Figure 7.

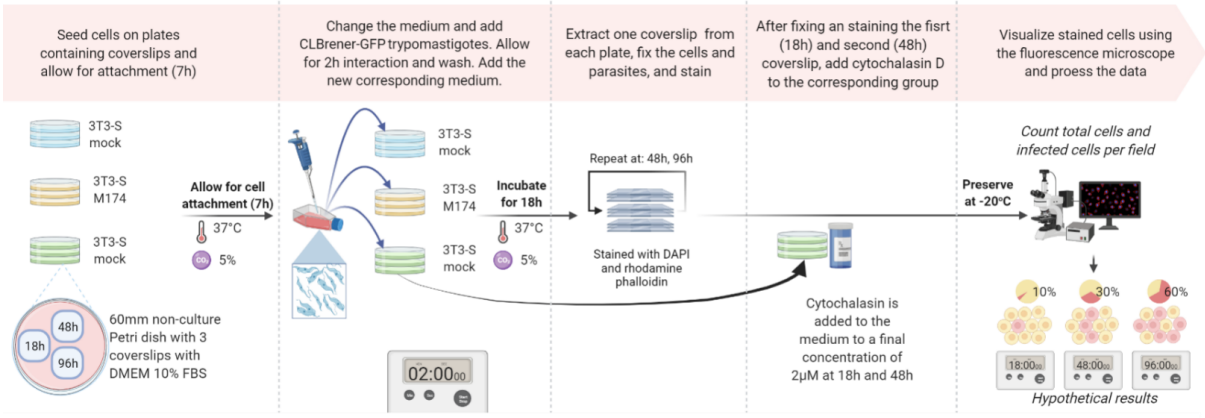

Figure 7: Schematic illustration of the experiment evaluating the potential role of filamentous actin in cell-to-cell transfer. Designed using Biorender.com

Mathematical models

The aim was to estimate mathematically the probability of an infected cell to be next to another infected cell.

In a population of N cells with I of them infected, the probability of infection can be estimated as $p_I=I/N$. Both values were obtained from counting total and infected cells via epifluorescence microscopy of 25 fields (40x) for each replicate and time. It was also measured the average number of cells with which a cell is in contact, which was called n. This value (n) was obtained by counting the number of cells with which a cell was in contact in 25 cases. Taking this number into account, the probability that at least one of the cells surrounding an infected cell is infected is npI. For instance, if the percentage of infected cells was five percent ($pI=0.05$) and one cell is in contact with 6 cells on average ($n=6$), the probability of an infected cell being next to another infected cell will be around 0.3.

Results

Cell-growth rate inhibition

To inhibit the growth of the cells under study (3T3-S, 3T3-NIH and H9c2), we determined the IC50 (95% confidence interval (CI)) of Baicalein and Indisulam (cell-cycle arresting drugs) at 24h, 48h, and 72h, as described in Materials and Methods. To do this, we first established the experimental conditions to determine the cell growth, using the methylene blue method. The quality of this assay was determined by the linear correlation found between the light absorbance and the known cell concentrations. As shown in Figure 8, the coefficient of determination (R^2) for 3T3-S cells was 0.986, which is a strong correlation, while the R^2 value for 3T3-NIH cells was 0.618, which is a very weak correlation. In the case of H9c2 cells, the correlation is nearly not existing, being the R^2 value 0.158. Based on these results, it was determined that the methylene blue assay was only useful for 3T3-S cells, but not for the 3T3-NIH and H9c2 cells that were easily detached from the well. Therefore, only the 3T3-S cells were used for the next experiments.

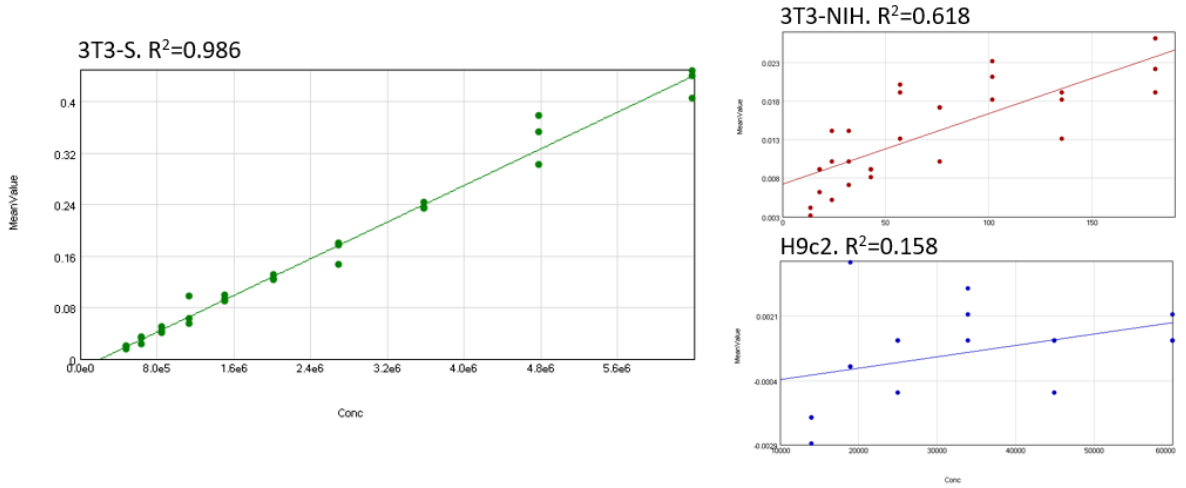

Figure 8: Scatter plots showing the relationship between the light absorbance from the methylene blue assay (y) and the number of seeded cells (x). A linear regression line was plotted fitting the empirical values. The coefficient of determination was calculated and annotated on the top of the graph.

Once the conditions for the cell growth quantification were established, the IC50 of Baicalein and Indisulam in the 3T3-S cells was determined. As shown in Figure 9, the dose-response curve determined that the IC50 (95% confidence interval (CI)) for Baicalein at 24h, 48h, and 72h are 20.01 (12.06-34.32) µM, 16.51 (10.34-26.81) µM, and 15.79 (9.94-25.80) µM, respectively. The IC50 values for different times are similar, decreasing slightly over time; and the 95% CIs are not very wide. Besides, it is observed how the optical density (cell number) decreases the higher the drug concentration is. Since the IC50 is lower over time, the drug could have an accumulative effect. It can also be noticed that the highest drug concentrations (40 and 80 µM) had a lethal effect on the cells, reducing the cell number to 0.

Moreover, the dose-response curve of Figure 10 shows that the IC50 (95% confidence interval (CI)) for Indisulam at 24h, 48h, and 72h are 76.29 (n.a.) µM, 0.774 (0.09-7.62) µM, and 1.739 (0.81-4.02) µM, respectively. The IC50 values for different times are very different between them and in the case of 24h the value is not precise enough. In addition, the 95% CIs are very wide. This can be seen in Figure 10, where there is no evident effect of the drug concentration

on the cell number at 24h and 48h. The value from the highest concentration (12 µM) is higher than the rest because of experimental error during the cell seeding. At 72h, it can be observed a reduction in cell number as the drug concentration increases, meaning that the drug might have a retarded effect. The summary of these results (Table 1) showed that Indisulam had no effect on cell growth, while baicalein at 16.51 µM reduced cell growth by 50%. Therefore, this last drug is the one used in the following experiments.

Table 1: Results from the dose-response curve of Baicalein and Indisulam at times 24h, 48h, and 72h. The table includes de calculated IC50, the Log value of IC50, and the 95% confidence interval.

TABLE OF RESULTS

BAICALEIN			
Time (h)	**IC50 (µM)**	**LogIC50**	**95% CI (IC50 (µM))**
24	20.01	1.301	12.06-34.32
48	16.51	1.218	10.34-26.81
72	15.79	1.199	9.939-25.80
INDISULAM			
Time (h)	**IC50 (µM)**	**LogIC50**	**95% CI (IC50 (µM))**
24	~ 76.288	~ 15.27	(very wide)
48	0.774	-0.1133	0.093-7.616
72	1.739	0.240	0.814-4.022

In the case of the experiment using DMEM with different FBS concentrations, the results are shown in Figure 11. It is observed that the cell number increases with higher FBS concentrations, and that this increase is more remarkable as time passes.

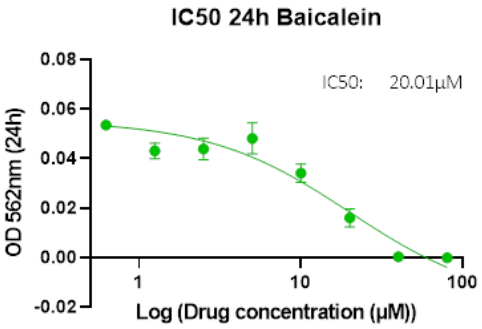

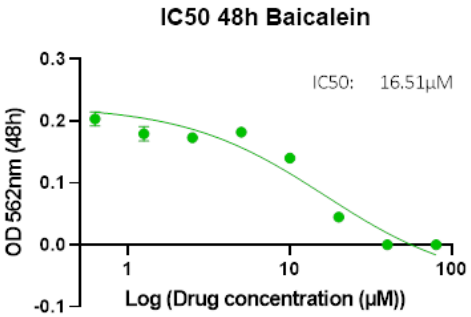

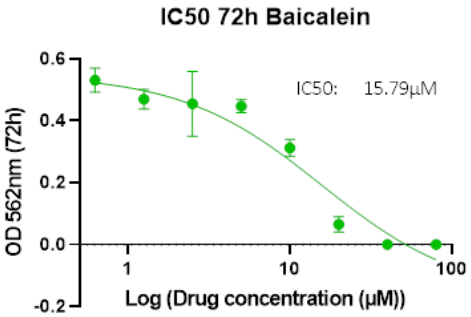

Figure 10: Dose-response curves for 3T3-S cells treated with Baicalein at concentrations of (µM): 80, 40, 20, 10, 5, 2.5, 1.25, y 0.625. The optical density (OD) is used as the cell number, based on the found correlation. Each graph corresponds to a different time point (24h, 48h, and 72h) and the calculated IC50 is displayed on the top right.

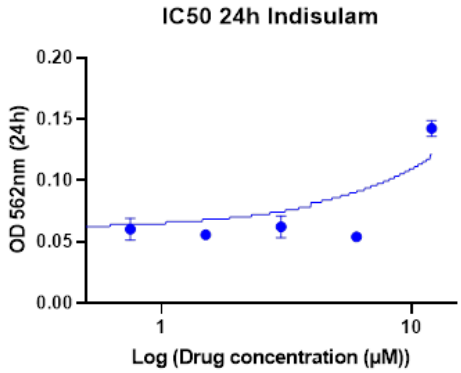

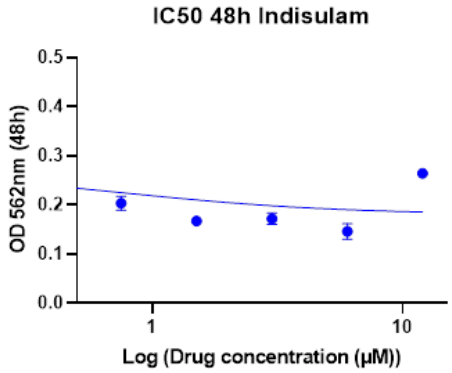

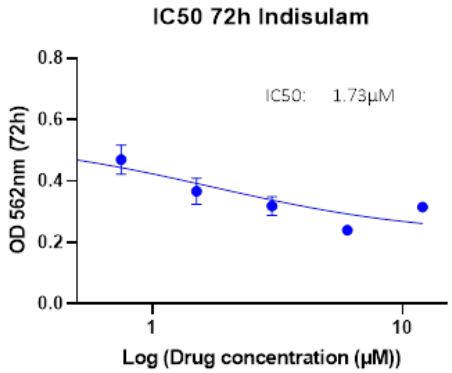

Figure 9: Dose-response curves for 3T3-S cells treated with Indisulam at concentrations of (µM 12, 6, 3, 1.5, 0.75). The optical density (OD) is used as the cell number, based on the found correlation. Each graph corresponds to a different time point (24h, 48h, and 72h) and the calculated IC50, when available, is displayed on the top right.

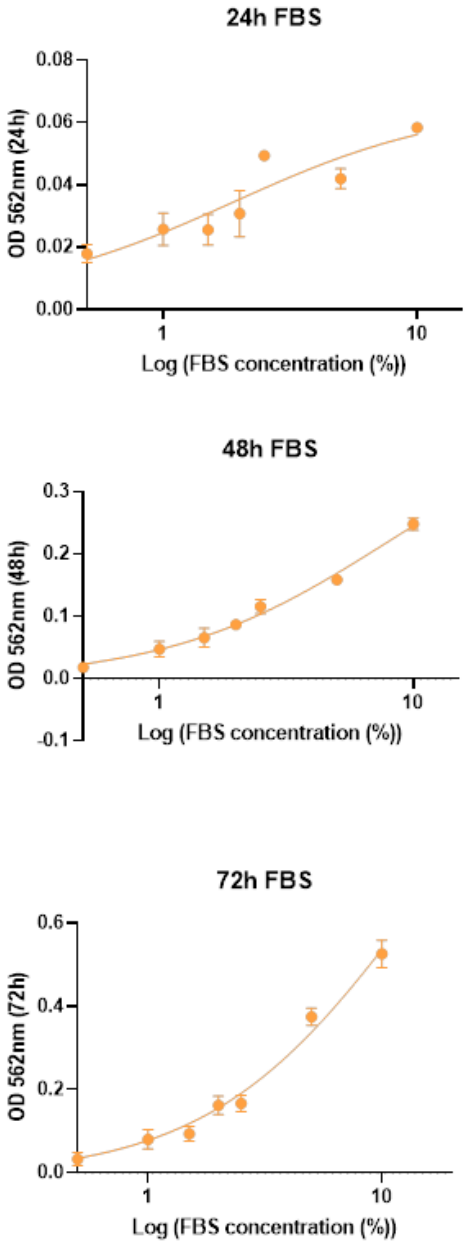

Figure 11: Dose-response curves for 3T3-S cells exposed to FBS concentrations of (%): 0.5, 1, 1.5, 2, 2.5, 5, 10. The optical density (OD) is used as the cell number. Each graph corresponds to each time point: 24h, 48h, 72h.

The combination effect on the cell growth of 3T3-S cells of FBS and Baicalein is shown in Figure 12. The concentration of Baicalein was the IC50 calculated at 48h:16.51µM. The number of cells was normalized by calculating the percentage of cells in relation to the control group (orange). In other words, the initial cell number of all groups was normalized to 0 and the cell numbers at other times were plotted as a percentage compared to the 100%, which was the value of the control group at 96h. This was done to overcome the difference in initial cell numbers, caused by the weaker adhesion of cells exposed to Baicalein or low FBS concentrations.

During the first 48h, the group treated with Baicalein gradually grew less. At 48h, the control group had cells at around 30%, whereas the group treated with Baicalein was at 15%, confirming the half-maximum inhibitory effect of the calculated IC50 concentration.

After 48h, the control group (orange) kept growing exponentially, as it was expected. On the other hand, the group grown in the absence of Baicalein but with a reduction of FBS to 2% after 48h (black), had a decrease in cell growth compared to the control (35% vs. 55% at 72h and 55% vs. 100% at 96h). In the case of the groups treated with Baicalein during 48h, the cells which were kept in the same conditions, DMEM 10% FBS and Baicalein (green) kept growing slightly more than half of the control group (orange). In the case of the group in which the medium was changed to DMEM 2% without the drug, the growth of the cells was significantly lower than the group with DMEM 10% + Baicalein (green). This shows that the effect of Baicalein is weaker than the effect of the reduction of FBS. The cells which were changed the medium to DMEM 2% + Baicalein (red), showed a reduced growth in comparison to the previously described case, meaning that the combination of FBS reduction and Baicalein might have an additive effect. This difference in cell number at 96h can be observed in Figure 13, where the statistical significance is shown.

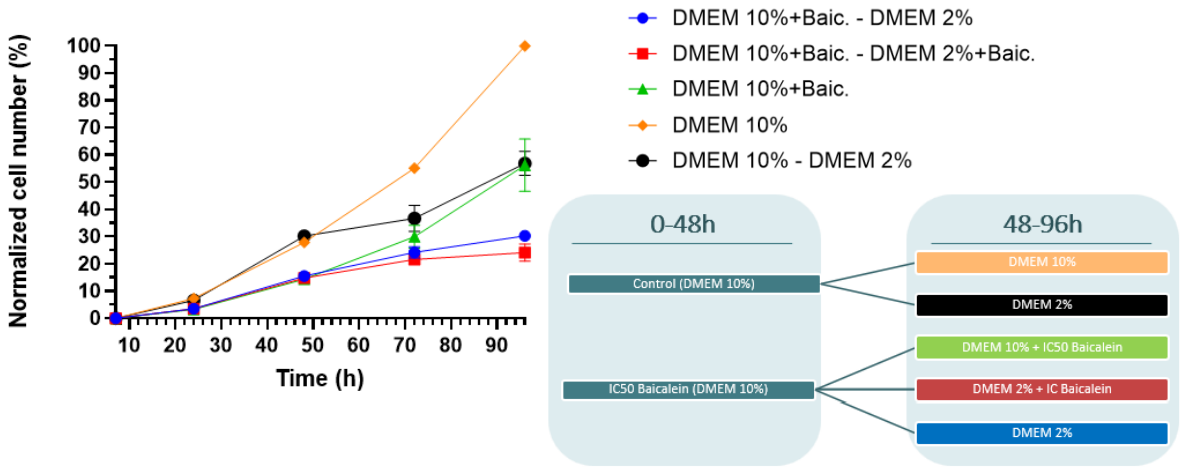

Figure 12:Growth curves of 3T3-S cells cultured with different conditions of FBS and Baicalein. Two groups of cells were seeded with DMEM supplemented with 10% of FBS in the absence or presence of the IC50 of Baicalein. At 48h, the medium was changed and DMEM with 10% FBS (orange) or DMEM with 2% FBS (black) was added to the cells that were in the absence of the drug; DMEM 10% + IC50 Baicalein (green), DMEM 2% + IC50 Baicalein (red) or DMEM 2% (blue) was added to the cells that were in the presence of the drug.

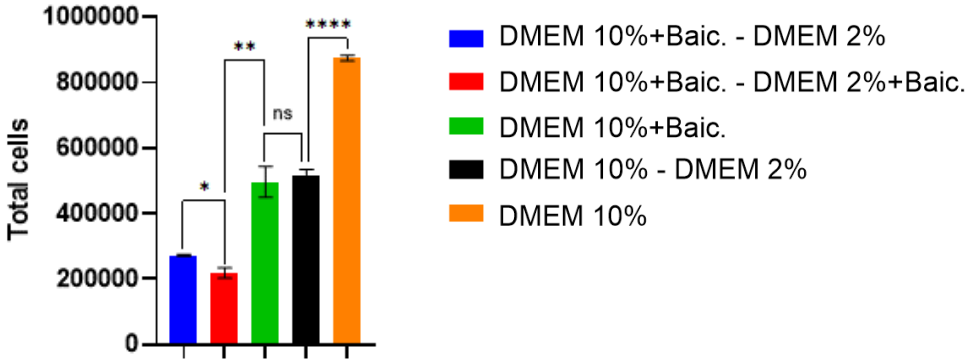

Figure 13: Total number of cells at 96h from the growth-curves using 3T3-S cells. The statistical comparison between the groups of interest was performed using t-tests. The p-values, from left to right, are: 0.0274, 0.0052 ,0.7595, <0.0001.

To know the effect alone of Baicalein on 3T3-S cell growth, the green and orange, and the black and red groups must be compared. From this comparison it can be observed that Baicalein does have an effect on the cell growth. To assess the effect alone of the reduction of FBS, the orange and black groups must be compared after 48h. According to the experiment, there is a significant reduction of cell-growth when FBS is reduced. If the combination of both the FBS reduction and Baicalein is to be analysed, the groups orange and red can be compared. According to this comparison, there is a significant difference in which the combination reduces more the cell growth than only FBS reduction (black) or Baicalein (green). Finally, if the effect of only a pre-treatment with Baicalein was to be investigates, the blue and red group had to be compared. In this case, it is shown that the variation between the groups when Baicalein is removed but the same FBS concentration is left is not very big, meaning that the effect of Baicalein could persist in cells after its removal.

To summarize, cell growth was inhibited by serum deprivation or using a drug arresting the cell cycle, namely Baicalein. It was decided that cells would be pre-treated for 48h before infection; so, when they were infected, cell-growth rate would have been already inhibited. For that reason, the IC50 of Baicalein at 48h was used. A constraint of the IC50 calculation was that cells exposed to high concentrations of drug attached less when seeded. Consequently, the initial number of cells was different for the high drug concentrations. To compensate for this variable, initial cell counts were normalized and the IC50 was calculated. It was also seen that serum deprivation, reducing FBS in medium from 10% to 2%, had a greater effect on the cell-growth rate than the IC50 of Baicalein.

Effect of cell-growth rate on *T. cruzi* invasion and infection

Figure 14 illustrates the results from the infectivity assays performed using 3T3-S cells with modified cell growth. Table 2 summarized the statistical analysis of the data for the percentage of infected cells.

In the graph F14.A, at 18h the control group (blue) and the group treated with Baicalein (red) have the same mean of percentage of infected cells, whereas the group pre-treated with DMEM 2% has approximately a doble mean of the percentage of infected cells. This tendency is similar for 48h, but not for 96h. At 96h, all the groups have a very similar percentage of infected cells. However, none of the observed differences as statistically significant when performing individual t-tests between with the control group (alpha=0.05). This could be done to the big standard error. Another observation is that the percentage of infected cells decreases during the first 96h of infection.

The graph F14.B considers the number of infected cells in 25 random microscope fields (40x) without calculating the percentage of infected cells. In other words, it is not taking into account the total cell number. This plot was used because the total cell number per field was distinct between the groups due to the modification in cell growth, and it could add a variable if infected cells did not divide at the same pace as non-infected cells. In this plot, there is no significant difference at 18h in the number of infected cells. However, at 48h, the group pre-treated with DMEM 2% presents a significantly higher number of infected cells. This tendency changes at 96h since all the groups have similar number of infected cells, with the control group being slightly higher. An important observation is that whereas the percentage of infected cells decreases over time, the total number of infected cells increases.

The graph F14.C shows the total number of cells per microscope field (40x) for every group and time. These values were used as an estimation of cell-growth rate. At 18h, the Baicalein group (red) and the control (blue) have the same cell number per field, whereas the group pre-treated with DMEM 2% (green) has a lower growth. This results are inverse to the percentage of infected cells at the same time, suggesting a potential correlation. At 48h, the group with the highest number of cells is the control group (blue), followed by the group treated with Baicalein (red), the group pre-treated with DMEM 2% having the lowest number of cells.

Table 2: Statistical summary for the percentage of infected 3T3-S cells.

	Positive control			*Baicalein IC50*			*Pre-treatment with DMEM 2%*		
	Mean	SEM	N	Mean	SEM	N	Mean	SEM	N
18h	0.363	0.042	3	0.398	0.092	3	0.848	0.350	3
48h	0.145	0.022	3	0.211	0.034	3	0.806	0.264	3
96h	0.181	0.010	3	0.155	0.039	3	0.223	0.054	3

A

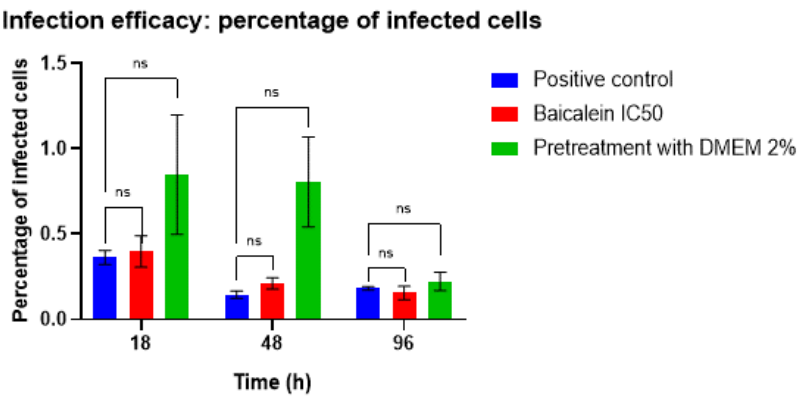

B

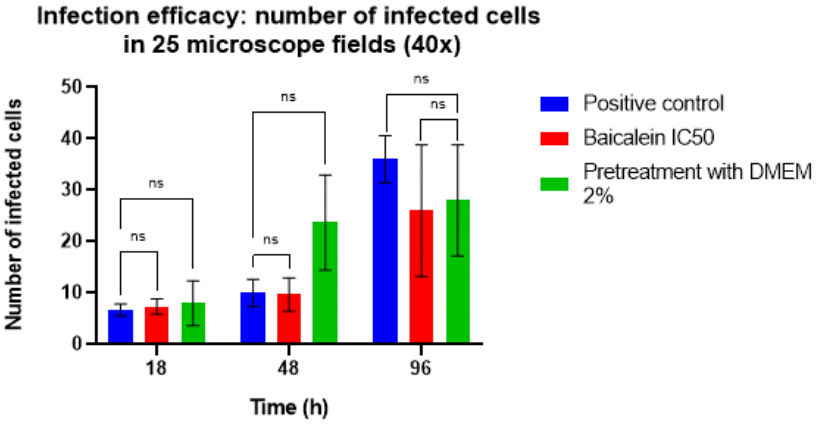

C

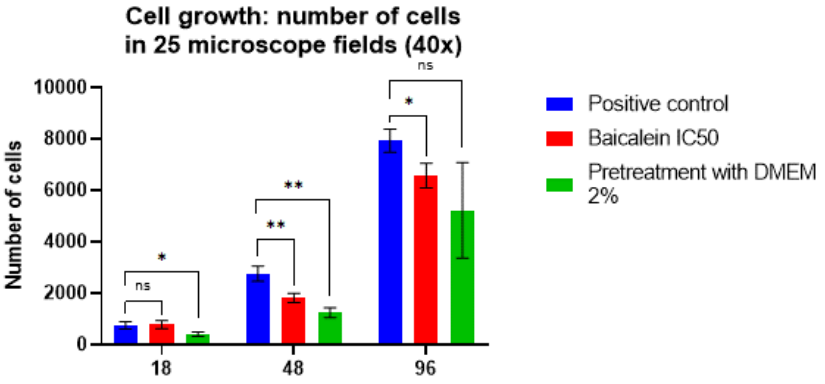

Figure 14: Invasion and infection efficiency of CL-Brener trypomastigotes in 3T3-S cells. The first graph (A) shows the percentage of infected cells (mean, SEM). The second graph (B) illustrates the number of infected cells in 25 aleatory microscope fields (40x), without considering the total number of cells (mean, SEM). The third graph (C) is an estimation of the cell-growth rate using the number of total cells per microscopic field (40x) at different times (mean, SEM). The groups are the control (blue), the cells pre-treated for 48h with DMEM 2% (green), and the group treated with the IC50 of Baicalein (16.51µM) (red). All the statistical analysis were t-tests. The p-values were non-significant (ns) if they were greater than 0.05. For the cell-growth graph (C), the p-values were, from right to left, 0.8237, 0.0252, 0.0090, 0.0018,

Since the sample size was small, a Shapiro-Wilcon test was performed to know if the data was normally distributed. All p values were greater than 0.11 (alpha value 0.05), so the null hypothesis that the data is normally distributed could not be rejected. Then, a two-way ANOVA test was performed for the percentage of infected cells, having as variables time and treatment. The results from this test can be found in Table 3. In summary, a statistically significant difference was found between treatments (p=0.0145). However, a two-way ANOVA test for the number of infected cells in 25 microscope fields (40x) was also performed (Table 4) and there was only a significant difference between time points, but not treatments (p=0.0005 and p=0.1767, respectively). If we performed individual t-tests for the treatments, only the group pre-treated with DMEM 2% at 48h had a significant difference (one-tailed, p value=0.0335*).

Table 3: Two-way ANOVA test for the percentage of infected 3T3-S cells having as variables time and treatment. Times: 18, 48h, 96h. Treatments: Control, Baicalein IC50, and pre-treatment with DMEM 2%. Threshold for statistical significance: 0.05. The values for the percentage of infected cells were obtained from counting the total and infected cells of 25 microscope fields (40x) for each replicate (3) in every treatment and time.

Two-Way ANOVA test – Percentage of Infected cells 3T3-S					
Factor	Degrees of Freedom	Sums of squares	Mean square	F-value	P-value
Time	2	0.5546	0.2773	3.451	0.0977
Treatments	2	0.8852	0.4426	9.312	0.0145 (*)

Table 4: Two-way ANOVA test for the total number of infected 3T3-S cells in 25 microscope fields (40x), having as variables time and treatment. Times: 18, 48h, 96h. Treatments: Control, Baicalein IC50, and pre-treatment with DMEM 2%. Threshold for statistical significance: 0.05. The assessed means values were the count of infected cells in 25 microscope fields for every replicate (3) in each time and treatment.

Two-Way ANOVA test – Total Infected Cells in 25 Microscope Fields (40x) 3T3-S					
Factor	Degrees of Freedom	Sums of squares	Mean square	F-value	P-value
Time	2	2419	1209	21.48	0.0005 (***)
Treatments	2	140.1	70.04	2.346	0.1767

Figure 15 illustrates the results from the infection assays realized in 3T3-NIH cells with modified cell-growth rate. In this case, there is only a control group and a group pre-treated for 48h with DMEM 2%.

In the graph F15.A, the percentage of infected cells at times 18h and 48h for both groups is shown. It can be observed that there is no significant difference between the groups nor the times (t-tests with p values greater than 0.05). This can be validated with the ANOVA test found in Table 5, which shows the p values for time (p=0.64) and treatment (p=0.787).

In the graph F15.B, the total cell count per microscope field (40x) is plotted. The control group (blue) has a higher cell number than the pre-treated group (red) at 18h and 48h, being this difference greater at 48h. The statical significance of this differences can be seen in the graph, with p values of 0.0285 and 0.0012, respectively.

A

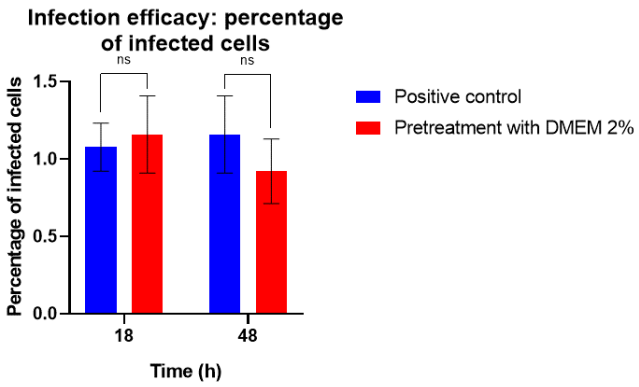

B

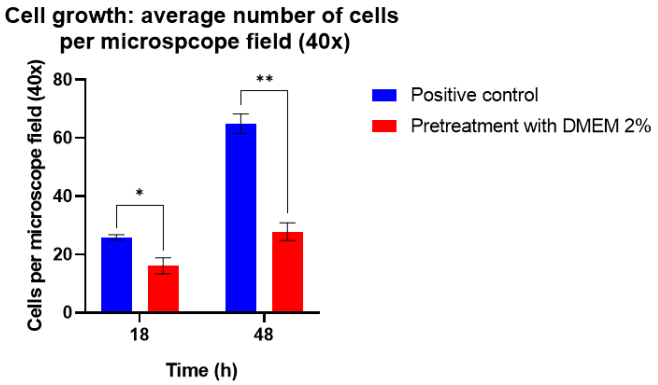

Figure 15: Invasion and infection efficiency of CL-Brener trypomastigotes in 3T3-NIH cells. The first graph (A) shows the percentage of infected cells (mean, SEM). The second graph (B) is an estimation of the cell-growth rate using the number of total cells per microscopic field (40x) at different times (mean, SEM). The groups are the control group (blue) and the cells pre-treated for 48h with DMEM 2% (red). The p-values for the cell-growth graph were, from left to right, 0.0285 and 0.0012.

Table 5: Two-way ANOVA test for the percentage of infected 3T3-NIH cells having as variables time and treatment. Times: 18, 48h, 96h. Treatments: Control and pre-treatment with DMEM 2%. Threshold for statistical significance: 0.05. The values for the percentage of infected cells were obtained from counting the total and infected cells of 25 microscope fields (40x) for each replicate (3) in every treatment and time.

Two-Way ANOVA test – Percentage of Infected cells 3T3-NIH					
Factor	Degrees of Freedom	Sums of squares	Mean square	F-value	P-value
Time	1	0.0181	0.0181	0.255	0.640
Treatments	1	0.0181	0.0181	0.083	0.787

Effect of Baicalein on epimastigotes

The results illustrated in Figure 16 show that there is no significant effect on epimastigote growth after 24h of Baicalein exposure. This was confirmed running a t-test, which gave a p-value of 0.102, meaning that there is no evidence for statistical difference. After 24h, both groups had a bit less than double of the initial parasite inoculum ($7.5 \cdot 10^6$ vs. 1.24 and 1.39 $\cdot 10^7$, respectively).

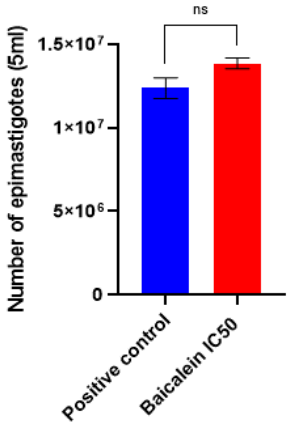

Figure 16: Number of epimastigotes after before and after 24h of exposure to Baicalein. The control group is shown in blue and the exposed group in red. P-value: 0.102.

Cell re-infection

The experiment infecting 3T3-NIH cells with half parasites transfected with the sequence coding for GFP and the other half for RFP aimed to observe if there was any cell infected with mixed parasites, meaning that it would have been re-infected. The analysed times were 24h and 48h. Over 50 microscope fields (20x) were analysed for each time, and all the infected cells were only infected with parasites expressing either the gene for GFP or RFP.

Probability of an infected cell to be next to another infected cell

As an estimation of short-range infections, such as cell-to-cell infection, it was determined whether infected cells were in direct contact with at least one more infected cell. Figure 17 shows the results from the analysis of 35 random 3T3-S infected cells. The statistical significance of Figure 17 was performed using t-tests and all the p-values were greater than 0.05. When this analysis was done using an ANOVA test (Table 6), there was no significant different in the percentage of infected cells in contact with other infected cells between the treatment groups (p=0.733). However, there was an increase of this percentage over time, which was statistically significant (p=0.0041**). In other words, as time passes more infected cells were in contact with infected cells.

The number of parasites per cell for 35 random 3T3-S cells is shown in Figure 18. Each dot corresponds to one cell. It can be observed that there is no significant different between groups (all p values greater that 0.05). In addition, even though there are cells with higher number of parasites in posterior times, the mean keeps being constant over time.

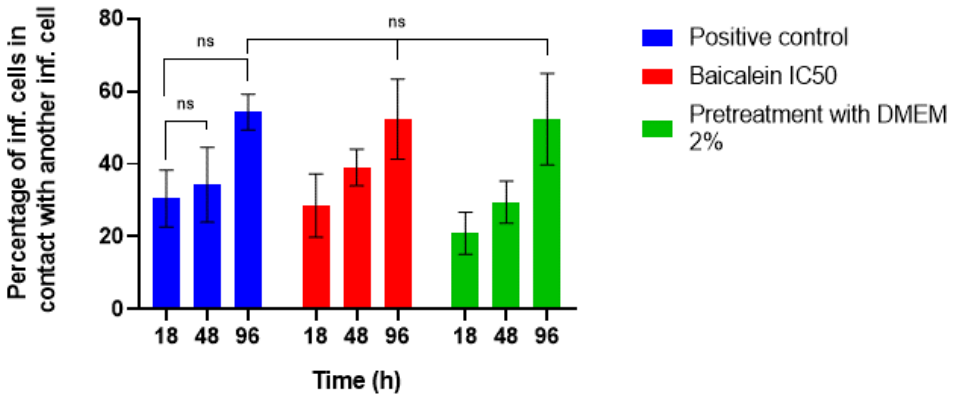

Figure 18: Percentage of infected 3T3-S cells in direct contact with one or more infected cells. The graph shows the results for 3 groups: control (blue), treated with IC50 of Baicalein (red), and pre-treated with DMEM 2% (green).

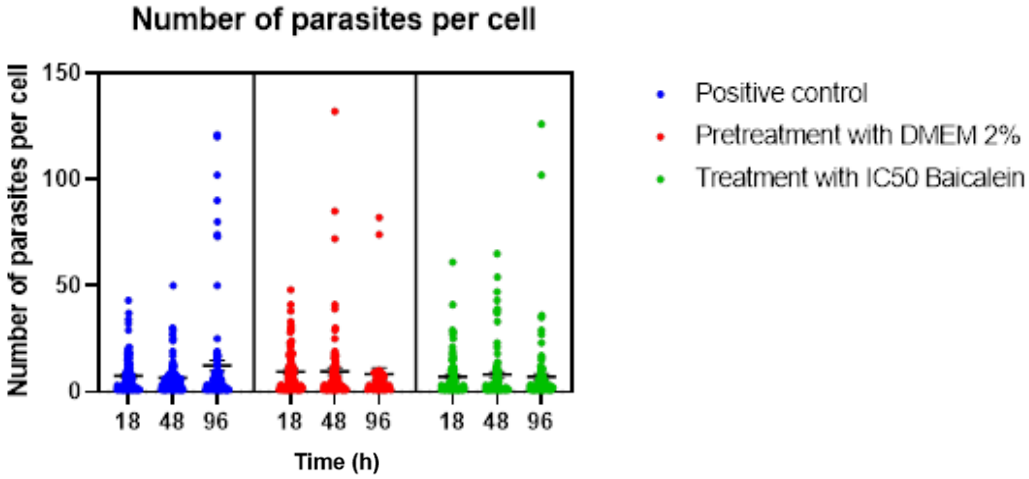

Figure 17: Number of parasites per cell. The number of parasites was counted in 35 random cells (3T3-S). Each dot corresponds to one cell.

Table 6: Two-way ANOVA test for the percentage of infected cells in contact with other infected cells (3T3-S). Variables: time and treatment. Times: 18, 48h, 96h. Treatments: Control, IC50 of Baicalein, and pre-treatment with DMEM 2%. Threshold for statistical significance: 0.05. The values for the percentage of infected cells in contact with an infected cell were obtained from analysing 35 random cell in each replicate (3) in every treatment and time.

Two-Way ANOVA test – Percentage of Infected cells 3T3-NIH					
Factor	Degrees of Freedom	Sums of squares	Mean square	F-value	P-value
Time	2	3309	1655	9.292	0.0041
Treatments	2	185.6	92.82	0.327	0.737

In order to know if the percentage of infected cells in contact with other infected cells was a random event, the stochastic probability was calculated. In Table 7, it is displayed the percentage of infected cells (*pI*), the average number of cells with which a cell is in contact (*n*), the probability of an infected cell being next to another infected cell (p_{Icon}), and the percentage of infected cells in contact with infected cells (*pIcon*). The used data is obtained from the control 3T3-S group, since no significant differences were found between the other groups. The values for *pI, n* and the percentage of infected cells in contact with infected cells were calculated empirically from the data from the infectivity assays. The probability of an infected cell to be next to another infected cells is a mathematical calculation from multiplying *n* and *pI.*

Table 7: Percentage of infected cells (pI), average number of cells with which a cell is in contact (n), the probability of an infected cell being next to another infected cell (p_{IC}) -mathematical-, and the percentage of infected cells in contact with infected cells (pIC) -empirical-. The values are the mean ± standard deviation.

Control group: 3T3-S	***pI***	***n***	***pIcon (empirical)***	***p_{Icon} (theoretical)***
18h	0.352 ± 0.060	1.72 ± 1.040	27.08 ± 11.02	0.00605
48h	0.139 ± 0.032	4.04 ± 1.148	25.95 ± 14.57	0.00561
96h	0.180 ± 0.0146	7 ± 1.058	53.36 ± 7.00	0.0026

In Table 7, the percentage of infected cells reduces over time, as it was mentioned above. The number of cells with which a cell is in contact increases over time, from 1.72 to 7, which is the expected result since the confluence of cells increases. The percentage of infected cells in contact with at least one more infected cell also increases from 18h to 96h, from 27.08 and 25.95 to 53.36. However, this value differs greatly from the calculated probability of an infected cell being next to another infected cell if this was a stochastic event. All probability values are >0.015. In other words, the calculated probability of an infected cell to be inContact with another infected cell is much lower than the percentage observed from the empirical data.

Potential role of filamentous actin on cell-to-cell transfer

To determine if filamentous actin played a role in the formation of clusters of infected cells, cytochalasin D and cells with a mutation in the actin gene were used. The experiment using cytochalasin D did not succeed because the exposure was probably too long. At 48h, there was a lot of detached cells and cell debris, meaning that cells were dying, which made this group not comparable to the control. Therefore, the results from this assay were not assessed. For the experiment with the actin-mutant cells, Table 8 shows the results from the infection assay at time 18h. The percentage of infected cells is lower for the mutant cells (3T3-S-M174). The number of cells with which a cell is in contact is very similar between the two groups, indicating that the confluence at that time was the same for both. The percentage of infected cells in contact with at least one more infected cell is higher for the control group, meaning that the mutant cells form less clusters of infected cells. In both cases, the obtained percentage is much higher than the calculated probability of an infected cell being next to another infected cell if this was a stochastic event. The probability value was higher for the control group, since the percentage of infected cells was also higher (Table 8).

Table 8: Percentage of infected cells (pI), average number of cells with which a cell is in contact (n), the probability of an infected cell being next to another infected cell (p_{IC}) -mathematical-, and the percentage of infected cells in contact with infected cells (pIC) -empirical-. The assessed time was 18h. The values are the mean ± standard deviation.

Time: 18h	***pI***	***n***	***pICon (empirical)***	***p_{Icon} (theoretical)***
3T3-S-MOCK	1.032 ± 0.280	1.6 ± 0.894	9.523 ± 5.387	0.0165
3T3-S-M174	0.385 ± 0.437	1.88 ± 0.765	1.905 ± 2.694	0.0072

Microscopy images assessing cell-to-cell infection

Fluorescence images supporting the formation of infected-cell clusters were taken. In addition, parasites potentially passing from one cell to another were also carefully analysed through fluorescence and confocal microscopy. Clusters of infected cells were found in all infections, even if the percentage of infected cells was very low and many microscope fields did not have any infected cells. Figure 19 and 20 show clusters of 3T3-S infected cells at 18h and 96h, respectively. In Appendix 1, Figures S1 and S2 are 3T3-NIH 48h after infection also showing clusters of infected cells, suggesting that it is not a cell-line specific characteristic. Figure S1 shows three infected cells, two of them in close contact with a very similar number of parasites and the same stage of infection. In Figure S2 it can be seen a cluster of 6 or 7 infected cells.

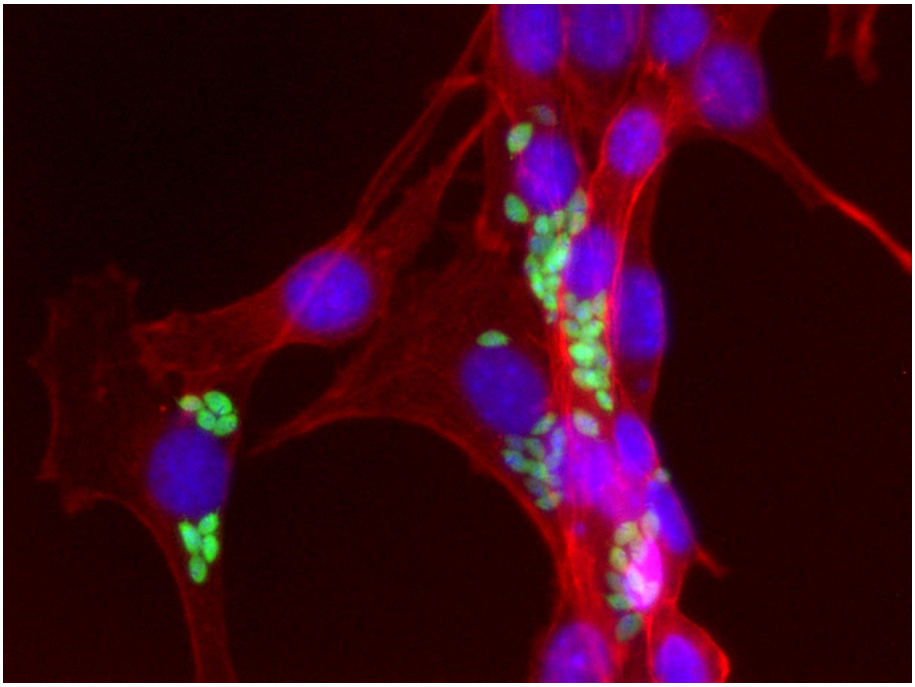

Figure 19: Cluster of infected 3T3-S cells at 18h. Green: parasites (GFP); red: filamentous actin (phalloidin rhodamine), blue: nucleus (DAPI). Epifluorescence microscope (40x)

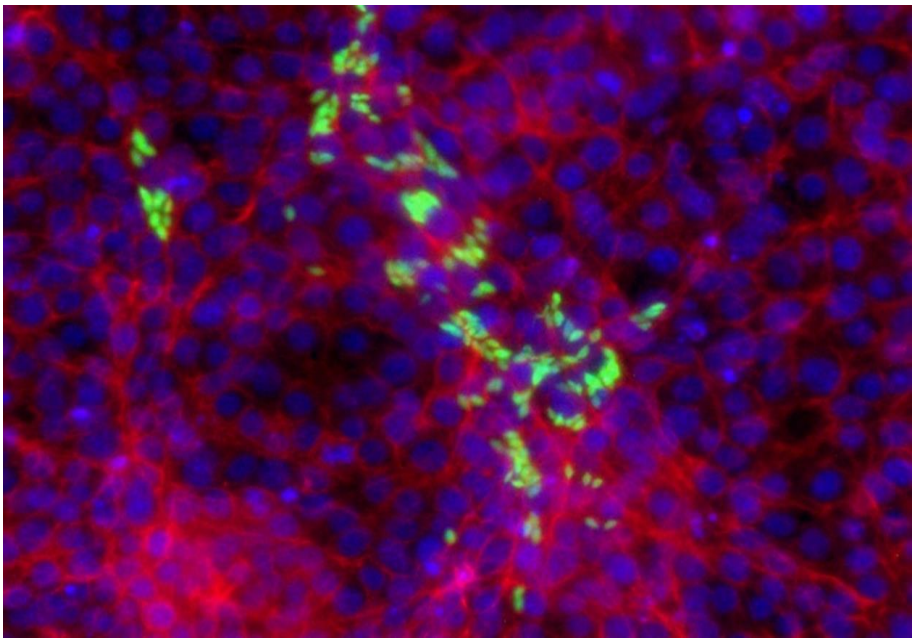

Figure 20: Cluster of infected 3T3-S cells 96h post infection. Green: parasites (GFP); red: filamentous actin (phalloidin rhodamine), blue: nucleus (DAPI). Epifluorescence microscope (20x).

Infected cells were found to be able to divide, which was not confirmed previously. This could be another potential explanation of the formation of flusters of infected cells. In Figure 21, three cases of cells during or just after division are shown. As it can be observed, a characteristic of dividing cells is that they detach and become rounded. In the case of F22.A and F22.B, the nuclei are compacted, and in the case of F22.A, they are polarized towards each other. In the case of F22.C, the compaction of chromosomes can be observed. Another important observation is that the distribution parasites when cells divide is not equitable. In the case of F22.A and F22.C, one cell will have one parasite and the other none. For F22.A, one will get 6 and the other one 3.

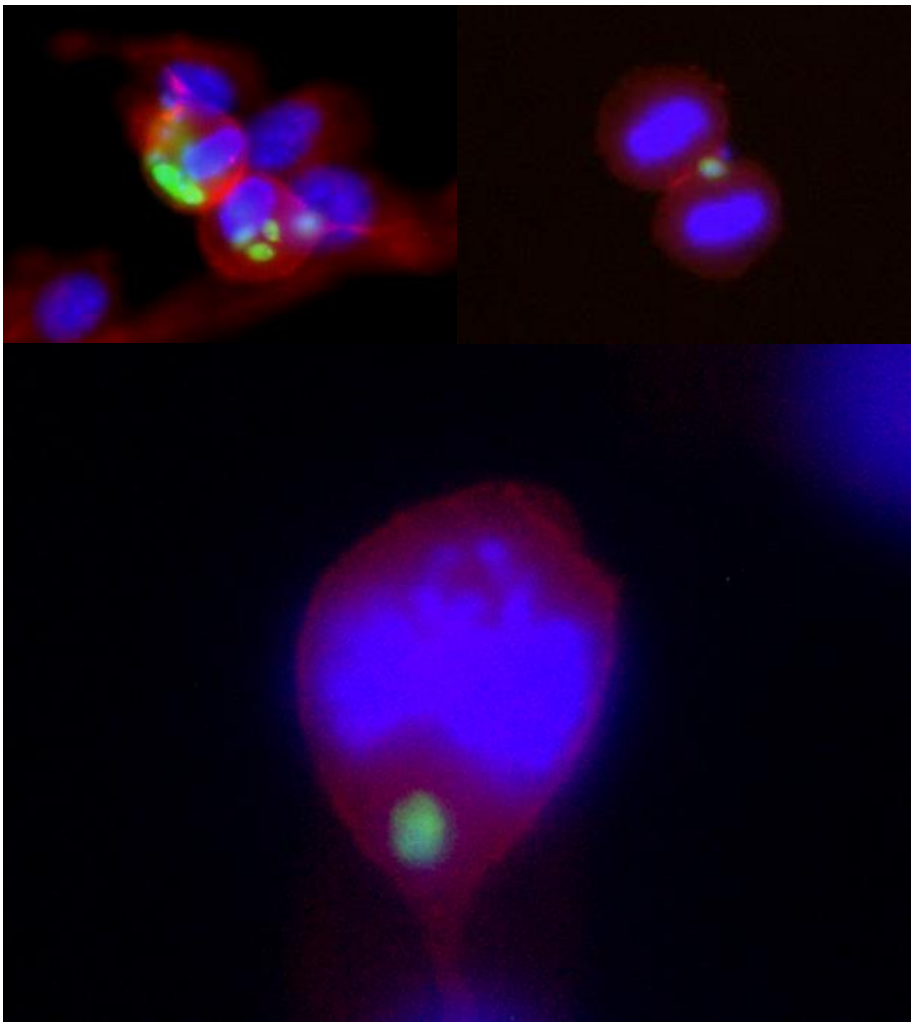

Figure 21: Suggestive images of infected cells during or just after cell division. Green: parasites (GFP); red: filamentous actin (phalloidin rhodamine), blue: nucleus (DAPI). Epifluorescence microscope (A and B 40x, C 80x)

Through fluorescence microscopy, a parasite was found suspected to be moving from one infected cell to the other cell (Appendix 1, Figure S3). These cells were then analysed with the laser confocal microscope to confirm that the parasite was inside the actin-cytoskeleton, and not just attached in the outside. Figure 22 shows a cross-section of the cells confirming that the parasite is inside the actin region and that there is an enriched actin area. In addition, it is noticed that there are also actin-enriched areas where the other parasites are located.
To further confirm this, Figure 23 shows a 3D model done from the confocal microscopy file of the section where the parasite of interest is found. Both images are taken from the opposite sides of the parasite, and it can be observed that in both cases the parasite is surrounded by filamentous actin. To further validate this, Figure S4 (Appendix 1) shows the same section but with the three fluorescent components independently. It is observed from this image that the regions where the parasite is found is enriched with filamentous actin.

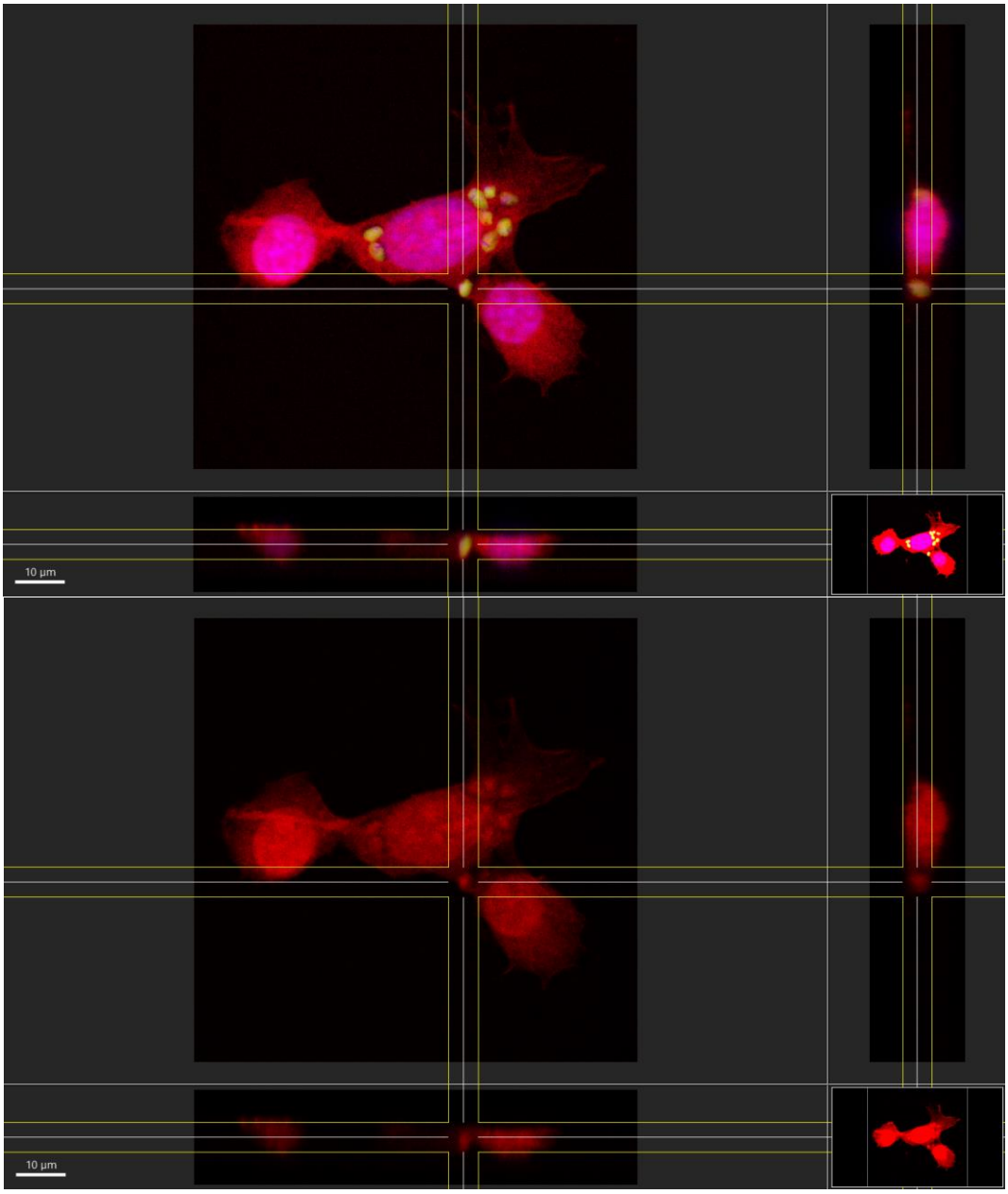

Figure 22: Cross-sections of the cells from Figure x taken by confocal microscopy. The top cross-section shows the merged composition (nucleus-DAPI, parasite-GFP, filamentous actin-phalloidin rhodamine) and the bottom cross-section only shows the filamentous actin (phalloidin rhodamine). From both images it is observed that the parasite is surrounded by actin cytoskeleton and that there is an enriched region of actin at its location. This is also the case for the other parasites.

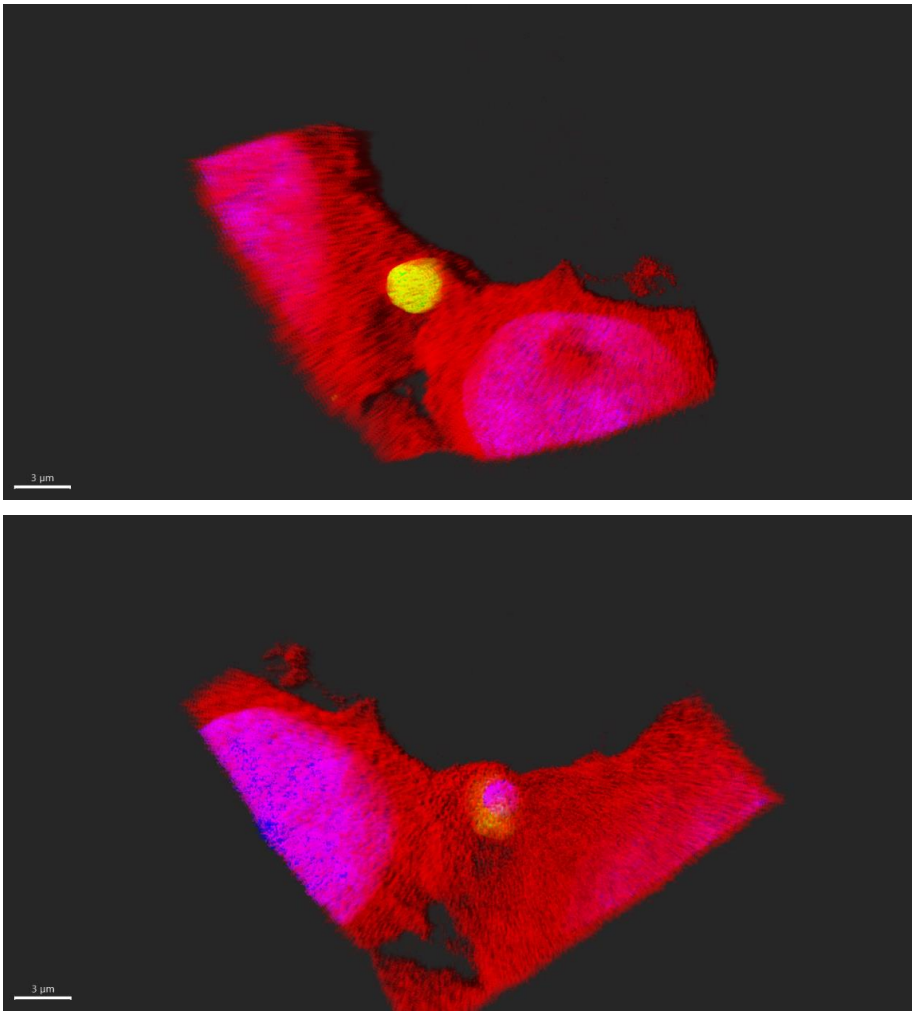

Figure 23: Magnification of the parasite potentially passing from one cell to the other. It is a 3D model made from the laser scanning confocal file. Each picture shows one side on the cells. The nuclei are blue, the actin cytoskeleton (filamentous actin) is red, and the parasite is green.

Discussion

Cell-growth rate reduction and invasion and infection efficacy

3T3-S cells pre-treated with DMEM 2% or treated with the IC50 of Baicalein to inhibit their growth rate. Then they were infected, and the percentage of infected cells was quantifies, in addition to the total number of infected cells in a certain number of microscope fields. The individual analysis between groups at each time showed non-statistically significant difference in any case. Suggesting that cell-growth rate does not affect invasion nor infection.
However, some differences could be appreciated even if they were not statistically significant. A reason for this could be the high standard error. In order to reduce this standard error and allow for more adequate statistical analysis, the sample size (N) should be bigger.

Something worth discussing is that the two-way ANOVA test for the percentage of infected cells (Table 3) showed a significant difference between groups but not time points. This significant difference is probably due to the increased percentage of infected cells for the group pre-treated with DMEM 2% at 18h and 48h. Interestingly, it was the opposite situation for the two-way ANOVA test of the total count of infected cells in 25 microscope fields (40x). In this case, the difference among groups was not significant, but the variation between time points was. The reasoning behind this difference is that the total count of infected cells does not consider the total number of cells. In other words, the total number of cells is distinct for each group due to the modification in cell-growth rate, but the number infected cells is the same. Consequently, the percentage of infected cells is lower for the groups with a higher total cell count. This also happens with the time points; even if the number of infected cells increases over time, the percentage diminished.

A possible explanation for this is that infected cells did not grow at the same pace. This could be due the parasite hijacking the cell metabolic pathways or competing for the same nutrients. In this case, non-infected cells would outgrow infected cells quicker in cases were the cell-growth rate is faster. For instance, the number of infected cells at 18h in 25 microscope fields is around 8-10 in every group, without any statistically significant difference. However, the percentage of infected cells does increase for the cells treated with DMEM 2%, which are also the cells with a lower total cell count. To know if the found difference in the percentage of infected cells is due to the difference in total cell count or in the efficiency of infection, the number of infected cells should be analysed at time 0h. This is very difficult empirically because most parasites are still in early stages of invasion, such as externally attached to the cells, and it can be difficult to identify the cells that are being infected. Therefore, the initial number of infected cells could be measured using a statistical model. If we assume that non-infected and infected cells grow exponentially, the number of cells would vary over time following equations 1 and 2, respectively (μ=cell-growth rate constant; I: infected cells; S: susceptible cells). If the experimental data is fitted into these equations, the μ_S and μ_I values can be estimated. This would allow to know the fraction of infected cells at earlier times following equation 3. If the percentage of initial infected cells is very low in comparison to total cells, as it was the case for this experiment, equation 4 would be used. The results from this project show that the fraction of infected cells ($F(t)$) diminishes over time. Therefore, it can be confirmed that $\mu_S > \mu_I$. In other words, the population of infected cells grows at a slower pace than susceptible cells in this experiment.

$$S(t) = S_0 e^{\mu_S t} \quad (1)$$

$$I(t) = I_0 e^{\mu_I t} \quad (2)$$

$$F(t) = \frac{I(t)}{S(t)+I(t)} = \frac{I_0 e^{\mu_I t}}{S_0 e^{\mu_S t} + I_0 e^{\mu_I t}}. \quad (3)$$

$$F(t) \approx \frac{I(t)}{S(t)} = \frac{I_0}{S_0} e^{(\mu_I - \mu_S)t} = F_0 e^{(\mu_I - \mu_S)t}. \quad (4)$$

In addition, an increase in infection efficacy in cells pre-treated with DMEM 2% could be due to autophagy. Serum deprivation induces autophagy in cells as a stress reaction. Autophagy is known to play a role in *T. cruzi* invasion, so the increase of autophagic cells due to pre-treatment with DMEM 2% could influence infection efficacy. Romano at al. (2009) described for the first time that the host-cell autophagic pathway played a crucial role in the lysosomal dependent entry of *T. cruzi*[56]. Interruption of mammalian autophagy reduced *T. cruzi* infectivity, whereas induction had the opposite effect [55,56]. However, in-vivo studies in mice showed the opposite result, probably because autophagy participates in the innate immune response by abducting intracellular pathogens and degrading them into autolysosomes, a process called xenophagy[54]. However, even if serum deprived 3T3-S cells were infected more during the first 48h, 3T3-NIH cells pre-treated with DMEM 2% did not show any difference in infection efficacy at 18h nor at 48h.

In conclusion, no evidence of cell-growth rate influencing the efficiency of invasion nor infection was found. Suggesting that the negative correlations found between the cell-growth rate of different cell lines and the infection efficacy by Arias-del-Angel et al. (2020)[57] could be random or caused by another variable. However, further data analysis and experiments should be performed in order to confirm these results.

Cell-to-cell infection

Cell-to-cell infection is a mechanism that allows many intracellular pathogens to establish successful infections avoiding exposure to the immune system, including *Leishmania spp.*, a a closely-related protozoan. This event has never been documented for *T. cruzi*. However, recent work proposed this mechanism via a mathematical model of the infection kinetics. This project aimed to investigate if amastigotes and/or trypomastigotes could pass from one cell to the other. Interestingly, infected cells were found to form clusters. In other words, groups of infected cells were found even when the percentage of infected cells was very low. This is a behaviour characteristic of short-range infections, such as cell-to-cell transmission. Therefore, to determine whether those clusters were a random event or not, statistical studies were done. They showed that the probability of an infected cell being in contact with another infected cell if this was a stochastic event was much lower than the empirically found probability. Meaning that this is not a random event and that short-range infections are a predominant mechanism.

There are two potential explanations to the clusters of infected cells: a) parasites pass from one cell to another, or b) infected cells divide and daughter cells attach close by. Both of this hypothesis are supported by the fact that the mean of parasites per cell over time was the same, even though it was expected to increase. In addition, the experiment infecting cells with both parasites transfected with the genes coding for GFP and RFP showed that no cells were infected

with both at the same time and that clusters were from one colour. In other words, cell re-infection was not observed, and the infected cells in the clusters had the same origin. This could be the case of both cell-to-cell transmission and infected cells dividing. In addition, if cell-to-cell transfer occurred, it would mean that parasites only pass to non-infected cells.

Another characteristic from the infected cells in contact is that the number of parasites was not always the same. In the case of cell-to-cell transmission, this could be the case if this event was occurring after amastigote replication. For instance, if a cell had 10 parasites and one of them moved to the neighbouring cell, one cell would have 9 parasites and the other one only one. This gap would probably increase once the parasites start dividing. Even though it was observed that the distribution of parasites in dividing cells was not equitable, the difference in parasite count should be smaller than the one observed if it was due to cell-to-cell transfer. In other words, if an infected cell was dividing the probability that the daughter cells have similar parasite counts is high. One approach to determine the probability of parasite distribution in dividing cells is to use a model assuming that parasites follow a binomial distribution with a success probability of 0.5. This is commonly used to determine plasmid distribution in dividing bacteria. If only pairs of infected cells in contact were analysed and the binomial distribution formula (equation 5) was used, the parasite distribution could be calculated following equation 6 (n_i: parasites in cell *I*; n_j: parasites in cell *j*). The closer to 0 the mean of the values from equation 6 is, the more uniform is the parasite distribution. If the mean was 10 or higher, the distribution of parasites would be too variable between two cells, meaning that the dominant mechanism would most likely be cell-to-cell transfer.

$$np(1-p) \tag{5}$$

$$\frac{(n_i-n_j)^2}{4(n_i+n_j)} \tag{6}$$

Via fluorescence microscopy, infected cells were inspected in search of parasites that could be moving from one cell to the other. Then, the most suggestive cases were carefully visualized through the laser scanner confocal microscope. Many of them were discarded because the 3D perspective confirm that they were not in the interface between cells, but inside of one of them. The most suggestive case, presented in the results, was an amastigote in between two cells, one of them infected with eight amastigotes. Both cells were connected via an actin-interface, where the parasite was found. To further confirm if this event is happening, it would be needed to record a time-lapse while the parasite is being transferred. This, however, is not easy because it is not known when does this event happen, how frequent it is, whether it happens with amastigotes, trypomastigotes or both, and if there is a special circumstance that triggers it, such as apoptosis signals. For instance, both *Cryptococcus* and *Leishmania* are transferred from one macrophage to another when this first one starts apoptosis, avoiding their release into the medium and subsequent exposure to the immune system once the cell lyses[64,68]. Another approach could be marking with antibodies proteins that are present during internalization, as it could be expected that parasites moving cell-to-cell undergo the same process as newly internalized parasites from the extracellular medium. A potential candidate could be Lysosome-associated membrane proteins 1 and 2 (LAMP 1-2). They are present at the parasitophorous vacuole membrane and in immunomodulatory LAMP-rich parasitophorous extrusions that mediate cell-to-cell transfer of *Leishmania amazonensis* amastigotes[67]. Cell-to-cell transfer of *T. cruzi* could also be tested by blocking its mechanism. Even though it is not

known if this is the case of *T. cruzi*, many intracellular pathogens hatch the host cell cytoskeleton, specifically actin, to pass from one cell to the other[58,62,64,67,68].

This project aimed to study the potential implication of actin in *T. cruzi* cell-to-cell transfer by either staining filamentous actin with rhodamine phalloidin or by diminishing actin polymerization using cytochalasin D or actin mutant cells. By staining filamentous actin, an actin-rich region was found at the location of the parasite that was potentially moving from cell-to-cell. In addition, cell-to-cell interactions were modulated by filamentous actin, which would most likely be needed for cell-to-cell parasite transfer. In the case of inhibiting actin polymerization using cytochalasin D, the experiment did not succeed. The reason behind this is that the exposure to cytochalasin D was too long for the cells to resist. The lack of filamentous actin probably interfered with many of their basic function, such as cell adhesion, increasing their detachment. Cytochalasin D treatment is usually very short because it tests time-specific questions, such as parasite internalization. However, it this experiment it was left for longer because it was not known when does cell-to-cell transfer occur. In addition, there is the possibility that this event happens with low frequency but over all the infection. Even with this limitations, cytochalasin D was tried because it gives the possibility to treat cells after parasite invasion. This is important because filamentous actin plays a key role in many of the parasite internalization pathways[81]. As an alternative to this experiment, cells with a mutation at the actin gene were used. This mutation interfered with actin polymerization, reducing the amount of filamentous actin in the cell. The downside of this approach is that actin polymerization was modified from the beginning of the infection, reducing the invasion efficiency of the mutant cells in comparison to the control group. However, the percentage of infected cells in contact with other infected cells was found to be five times lower for mutant cells. This could be due to less mutant cells being infected, but the mathematical calculated probability showed that if this was the case the percentage should be reduced by half, not by five. In addition, due to time constraints, time 48h and 96h could not be assessed, which could add information if the gap of cells clusters kept increasing between actin-mutant and control cells. However, it is important to keep in mind that the percentage of infected cells in contact with other infected cells is an estimation of short-range infections. Which also includes infected cells dividing.

An approach to know if the percentage of infected cells in contact is cause by infected cells dividing, cells transfected with fluorescent proteins could be added to a culture of non-transfected cells in a proportion equal to the percentage of infected cells, and the probability of them being in contact could be assessed. If it is the same as for the one found in the infections, then, most likely, the reason of the formation of infected-cell clusters would be cell division.

In conclusion, to confirm that cell-to-cell transfer occurs during *T. cruzi* infections, several experiments must prove it. In this project, many suggestive results indicate that it is possible and likely, which adds to the mathematical suggestion proposed by Arias-del-Angel et al. (2020)[57]. However, more experiments are needed to confirm it, such as time-lapse real time imaging.

In conclusion, this project aimed to determine whether cell-growth rate was a cellular characteristic influencing the infection efficiency of *T. cruzi*. The results showed no evidence to confirm this hypothesis, but more work in other cell lines, longer infection times, and bigger sample sizes should be performed to confirm these results. In addition, there is still the need to find the cellular characteristics that enhance *T. cruzi* infection efficacy, in order to understand the pathogenesis of the disease and find druggable targets. This study also proposes cell-to-cell infection as a possible explanation to the establishment of the disease. If this mechanism was used by *T. cruzi* it would allow the parasites propagate while avoiding the immune system, enhancing the probability of infection success. Therefore, it is of great importance to determine if this short-range mechanism is being used and, in case it is, in which conditions it occurs.

Acknowledgements

I would like to thank my supervisor Dr. Rebeca Manning Cela for her consistent support and guidance. In addition, I would also like to thank the rest of the research team for their collaboration during my stay in Mexico, especially Eloy Contreras. I would also like to acknowledge Moisés Santillan for providing advice regarding the mathematical approach. Also, a big thanks to Iván Galán who helped me use the confocal microscope. I am also thankful for my classmates at Uppsala University, who made my studying experience a great one. Finally, I would like to thank my family for their unconditional trust and love.

Bibliography

1. Center for Disease Control and Prevention. CDC - DPDx - American Trypanosomiasis. https://www.cdc.gov/dpdx/trypanosomiasisamerican/index.html (2021).
2. Chagas, C. Nova tripanozomiaze humana: estudos sobre a morfolojia e o ciclo evolutivo do Schizotrypanum cruzi n. gen., n. sp., ajente etiolojico de nova entidade morbida do homem. *Mem. Inst. Oswaldo Cruz* **1**, 159–218 (1909).
3. World Health Organization. Chagas disease (American trypanosomiasis). https://www.who.int/westernpacific/health-topics/chagas-disease (2021).
4. Lidani, K. C. F. *et al.* Chagas Disease: From Discovery to a Worldwide Health Problem. *Front. Public Health* **7**, 166 (2019).
5. Coura, J. R. & Viñas, P. A. Chagas disease: a new worldwide challenge. *Nature* **465**, S6–S7 (2010).
6. OPS. OPS/OMS | Información general: Enfermedad de Chagas. *Pan American Health Organization / World Health Organization* https://www3.paho.org/hq/index.php?option=com_content&view=article&id=5856:2011-informacion-general-enfermedad-chagas&Itemid=40370&lang=es (2021).
7. Engels, D. & Savioli, L. Reconsidering the underestimated burden caused by neglected tropical diseases. *Trends Parasitol.* **22**, 363–366 (2006).
8. Lee, B. Y., Bacon, K. M., Bottazzi, M. E. & Hotez, P. J. Global economic burden of Chagas disease: a computational simulation model. *Lancet Infect. Dis.* **13**, 342–348 (2013).
9. Conteh, L., Engels, T. & Molyneux, D. H. Socioeconomic aspects of neglected tropical diseases. *The Lancet* **375**, 239–247 (2010).

10. Grimwood, K., Lambert, S. B. & Milne, R. J. Rotavirus infections and vaccines: burden of illness and potential impact of vaccination. *Paediatr. Drugs* **12**, 235–256 (2010).
11. Cordovez, J. M. *et al.* Is vectorial transmission of Trypanosoma cruzi an efficient route to support high infection rates in sylvatic hosts? 860189 (2019) doi:10.1101/860189.
12. Rojas-De-Arias, A. Chagas disease prevention through improved housing using an ecosystem approach to health. *Cad. Saude Publica* **17 Suppl**, 89–97 (2001).
13. Bates, B. R., Villacís, A. G., Mendez-Trivino, A., Mendoza, L. E. & Grijalva, M. J. Determinants of intentions to prevent triatomine infestation based on the health belief model: An application in rural southern Ecuador. *PLoS Negl. Trop. Dis.* **14**, e0007987 (2020).
14. de Araújo, C. N., Bussacos, A. C., Sousa, A. O., Hecht, M. M. & Teixeira, A. R. L. Interactome: Smart hematophagous triatomine salivary gland molecules counteract human hemostasis during meal acquisition. *J. Proteomics* **75**, 3829–3841 (2012).
15. Sant'Anna, M. R. V., Soares, A. C., Araujo, R. N., Gontijo, N. F. & Pereira, M. H. Triatomines (Hemiptera, Reduviidae) blood intake: Physical constraints and biological adaptations. *J. Insect Physiol.* **97**, 20–26 (2017).
16. Leyria, J., Orchard, I. & Lange, A. B. What happens after a blood meal? A transcriptome analysis of the main tissues involved in egg production in Rhodnius prolixus, an insect vector of Chagas disease. *PLoS Negl. Trop. Dis.* **14**, e0008516 (2020).
17. Pietrokovsky, S., Bottazzi, V., Schweigmann, N., Haedo, A. & Wisnivesky-Colli, C. Comparison of the blood meal size among Triatoma infestans, T. guasayana and T. sordida (Hemiptera: Reduviidae) of Argentina under laboratory conditions. *Mem. Inst. Oswaldo Cruz* **91**, 241–242 (1996).

18. Reisenman, C. E., Gregory, T., Guerenstein, P. G. & Hildebrand, J. G. Feeding and Defecation Behavior of Triatoma rubida (Uhler, 1894) (Hemiptera: Reduviidae) under Laboratory Conditions, and Its Potential Role as a Vector of Chagas Disease in Arizona, USA. *Am. J. Trop. Med. Hyg.* **85**, 648–656 (2011).
19. Mosquera, K. D., Villacís, A. G. & Grijalva, M. J. Life Cycle, Feeding, and Defecation Patterns of Panstrongylus chinai (Hemiptera: Reduviidae: Triatominae) Under Laboratory Conditions. *J. Med. Entomol.* **53**, 776–781 (2016).
20. Villacís, A. G., Arcos-Terán, L. & Grijalva, M. J. Life cycle, feeding and defecation patterns of Rhodnius ecuadoriensis (Lent & León 1958) (Hemiptera: Reduviidae: Triatominae) under laboratory conditions. *Mem. Inst. Oswaldo Cruz* **103**, 690–695 (2008).
21. Martínez-Ibarra, J. A., Novelo López, M., Hernández Robles, M. del R. & Grant Guillén, Y. Influence of the blood meal source on the biology of Meccus picturatus Usinger 1939 (Hemiptera: Reduviidae: Triatominae) under laboratory conditions. *Mem. Inst. Oswaldo Cruz* **98**, 227–232 (2003).
22. Garg, N. J. Current global situation of Chagas disease. *Rev. Bioméd.* **32**, (2021).
23. Rassi, A., Rassi, A. & Marin-Neto, J. A. Chagas disease. *Lancet Lond. Engl.* **375**, 1388–1402 (2010).
24. Carter, Y. L., Juliano, J. J., Montgomery, S. P. & Qvarnstrom, Y. Acute Chagas Disease in a Returning Traveler. *Am. J. Trop. Med. Hyg.* **87**, 1038–1040 (2012).
25. Pinto, A. Y. das N., Valente, S. A., Valente, V. da C., Ferreira Junior, A. G. & Coura, J. R. [Acute phase of Chagas disease in the Brazilian Amazon region: study of 233 cases from Pará, Amapá and Maranhão observed between 1988 and 2005]. *Rev. Soc. Bras. Med. Trop.* **41**, 602–614 (2008).

26. Rincón-Acevedo, C. Y. *et al.* Clinical and Epidemiological Characterization of Acute Chagas Disease in Casanare, Eastern Colombia, 2012-2020. *Front. Med.* **8**, 681635 (2021).
27. Zingales, B. Trypanosoma cruzi genetic diversity: Something new for something known about Chagas disease manifestations, serodiagnosis and drug sensitivity. *Acta Trop.* **184**, 38–52 (2018).
28. Bastos, C. J. C. *et al.* Clinical outcomes of thirteen patients with acute chagas disease acquired through oral transmission from two urban outbreaks in northeastern Brazil. *PLoS Negl. Trop. Dis.* **4**, e711 (2010).
29. Issa, V. S. The Indeterminate Form of Chagas Disease. *Arq. Bras. Cardiol.* (2018) doi:10.5935/abc.20180027.
30. Coura, J. R., de Abreu, L. L., Pereira, J. B. & Willcox, H. P. [Morbidity in Chagas' disease. IV. Longitudinal study of 10 years in Pains and Iguatama, Minas Gerais, Brazil]. *Mem. Inst. Oswaldo Cruz* **80**, 73–80 (1985).
31. Cunha-Neto, E. & Chevillard, C. Chagas Disease Cardiomyopathy: Immunopathology and Genetics. *Mediators Inflamm.* **2014**, 683230 (2014).
32. Rassi, A., Rassi, A. & Marcondes de Rezende, J. American Trypanosomiasis (Chagas Disease). *Infect. Dis. Clin. North Am.* **26**, 275–291 (2012).
33. Pérez-Molina, J. A. & Molina, I. Chagas disease. *Lancet Lond. Engl.* **391**, 82–94 (2018).
34. De Bona, E. *et al.* Autoimmunity in Chronic Chagas Disease: A Road of Multiple Pathways to Cardiomyopathy? *Front. Immunol.* **9**, (2018).
35. WHO Expert Committee on the Control of Chagas Disease (2000 : Brasilia, B. & Organization, W. H. *Control of Chagas disease : second report of the WHO expert committee*. https://apps.who.int/iris/handle/10665/42443 (2002).

36. Brasil, P. E. A. A., De Castro, L., Hasslocher-Moreno, A. M., Sangenis, L. H. C. & Braga, J. U. ELISA versus PCR for diagnosis of chronic Chagas disease: systematic review and meta-analysis. *BMC Infect. Dis.* **10**, 337 (2010).
37. García-Huertas, P. & Cardona-Castro, N. Advances in the treatment of Chagas disease: Promising new drugs, plants and targets. *Biomed. Pharmacother.* **142**, 112020 (2021).
38. Martins, A. V. *et al.* Biology of Trypanosoma cruzi: An update. *Infectio* **16**, 45–58 (2012).
39. Ferri, G. & Edreira, M. M. All Roads Lead to Cytosol: Trypanosoma cruzi Multi-Strategic Approach to Invasion. *Front. Cell. Infect. Microbiol.* **11**, 634793 (2021).
40. Arias-del-Angel, J. A., Santana-Solano, J., Santillán, M. & Manning-Cela, R. G. Motility patterns of Trypanosoma cruzi trypomastigotes correlate with the efficiency of parasite invasion in vitro. *Sci. Rep.* **10**, 15894 (2020).
41. Onyekwelu, K. C. *Life Cycle of Trypanosoma cruzi in the Invertebrate and the Vertebrate Hosts*. *Biology of Trypanosoma cruzi* (IntechOpen, 2019). doi:10.5772/intechopen.84639.
42. Mule, S. N. *et al.* PhyloQuant approach provides insights into Trypanosoma cruzi evolution using a systems-wide mass spectrometry-based quantitative protein profile. *Commun. Biol.* **4**, 1–12 (2021).
43. Brenière, S. F., Waleckx, E. & Barnabé, C. Over Six Thousand Trypanosoma cruzi Strains Classified into Discrete Typing Units (DTUs): Attempt at an Inventory. *PLoS Negl. Trop. Dis.* **10**, e0004792 (2016).
44. Westenberger, S. J., Barnabé, C., Campbell, D. A. & Sturm, N. R. Two Hybridization Events Define the Population Structure of Trypanosoma cruzi. *Genetics* **171**, 527–543 (2005).

45. Freitas, J. M. de *et al.* Ancestral Genomes, Sex, and the Population Structure of Trypanosoma cruzi. *PLOS Pathog.* **2**, e24 (2006).
46. Zingales, B. *et al.* The revised Trypanosoma cruzi subspecific nomenclature: rationale, epidemiological relevance and research applications. *Infect. Genet. Evol. J. Mol. Epidemiol. Evol. Genet. Infect. Dis.* **12**, 240–253 (2012).
47. Tardieux, I. *et al.* Lysosome recruitment and fusion are early events required for trypanosome invasion of mammalian cells. *Cell* **71**, 1117–1130 (1992).
48. Rodríguez, A., Samoff, E., Rioult, M. G., Chung, A. & Andrews, N. W. Host cell invasion by trypanosomes requires lysosomes and microtubule/kinesin-mediated transport. *J. Cell Biol.* **134**, 349–362 (1996).
49. Woolsey, A. M. *et al.* Novel PI 3-kinase-dependent mechanisms of trypanosome invasion and vacuole maturation. *J. Cell Sci.* **116**, 3611–3622 (2003).
50. Fernandes, M. C., Flannery, A. R., Andrews, N. & Mortara, R. A. Extracellular amastigotes of Trypanosoma cruzi are potent inducers of phagocytosis in mammalian cells. *Cell. Microbiol.* **15**, 977–991 (2013).
51. Ferreira, B. L., Ferreira, É. R., Bonfim-Melo, A., Mortara, R. A. & Bahia, D. Trypanosoma cruzi extracellular amastigotes selectively trigger the PI3K/Akt and Erk pathways during HeLa cell invasion. *Microbes Infect.* **21**, 485–489 (2019).
52. Barrias, E., Reignault, L., de Carvalho, T. M. U. & de Souza, W. Clathrin coated pit dependent pathway for Trypanosoma cruzi internalization into host cells. *Acta Trop.* **199**, 105057 (2019).
53. Barrias, E. S., Reignault, L. C., De Souza, W. & Carvalho, T. M. U. Trypanosoma cruzi uses macropinocytosis as an additional entry pathway into mammalian host cell. *Microbes Infect.* **14**, 1340–1351 (2012).

54. Casassa, A. F., Vanrell, M. C., Colombo, M. I., Gottlieb, R. A. & Romano, P. S. Autophagy plays a protective role against Trypanosoma cruzi infection in mice. *Virulence* **10**, 151–165 (2019).
55. Salassa, B. N. & Romano, P. S. Autophagy: A necessary process during the Trypanosoma cruzi life-cycle. *Virulence* **10**, 460–469 (2019).
56. Romano, P. S., Arboit, M. A., Vázquez, C. L. & Colombo, M. I. The autophagic pathway is a key component in the lysosomal dependent entry of Trypanosoma cruzi into the host cell. *Autophagy* **5**, 6–18 (2009).
57. Arias-del-Angel, J. A., Manning-Cela, R. G. & Santillán, M. Dynamics of Mammalian Cell Infection by Trypanosoma cruzi trypomastigotes. *Front. Microbiol.* **11**, (2020).
58. Lamason, R. L. & Welch, M. D. Actin-based motility and cell-to-cell spread of bacterial pathogens. *Curr. Opin. Microbiol.* **35**, 48–57 (2017).
59. Ireton, K. Molecular mechanisms of cell–cell spread of intracellular bacterial pathogens. *Open Biol.* **3**, 130079 (2013).
60. Hagedorn, M., Rohde, K. H., Russell, D. G. & Soldati, T. Infection by tubercular mycobacteria is spread by nonlytic ejection from their amoeba hosts. *Science* **323**, 1729–1733 (2009).
61. Gerstenmaier, L. *et al.* The autophagic machinery ensures nonlytic transmission of mycobacteria. *Proc. Natl. Acad. Sci. U. S. A.* **112**, E687–E692 (2015).
62. Kespichayawattana, W., Rattanachetkul, S., Wanun, T., Utaisincharoen, P. & Sirisinha, S. Burkholderia pseudomallei induces cell fusion and actin-associated membrane protrusion: a possible mechanism for cell-to-cell spreading. *Infect. Immun.* **68**, 5377–5384 (2000).

63. Flieger, A., Frischknecht, F., Häcker, G., Hornef, M. W. & Pradel, G. Pathways of host cell exit by intracellular pathogens. *Microb. Cell* **5**, 525–544 (2018).
64. Alvarez, M. & Casadevall, A. Cell-to-cell spread and massive vacuole formation after Cryptococcus neoformans infection of murine macrophages. *BMC Immunol.* **8**, 16 (2007).
65. Ma, H., Croudace, J. E., Lammas, D. A. & May, R. C. Direct cell-to-cell spread of a pathogenic yeast. *BMC Immunol.* **8**, 15 (2007).
66. Ranatunga, M. *et al.* Leishmania aethiopica cell-to-cell spreading involves caspase-3, AkT and NF-κB but not PKC-δ activation and involves uptake of LAMP-1 positive bodies containing parasites. *FEBS J.* **287**, (2019).
67. Real, F. *et al.* Cell-to-cell transfer of Leishmania amazonensis amastigotes is mediated by immunomodulatory LAMP-rich parasitophorous extrusions. *Cell. Microbiol.* **16**, 1549–1564 (2014).
68. Rai, R., Dyer, P., Richardson, S., Harbige, L. & Getti, G. Apoptotic induction induces Leishmania aethiopica and L. mexicana spreading in terminally differentiated THP-1 cells. *Parasitology* **144**, 1912–1921 (2017).
69. Tartarelli, I. *et al.* During host cell traversal and cell-to-cell passage, Toxoplasma gondii sporozoites inhabit the parasitophorous vacuole and posteriorly release dense granule protein-associated membranous trails. *Int. J. Parasitol.* **50**, 1099–1115 (2020).
70. Fernandes, M. C. & Andrews, N. W. Host cell invasion by Trypanosoma cruzi: a unique strategy that promotes persistence. *FEMS Microbiol. Rev.* **36**, 734–747 (2012).
71. Silva Pereira, S., Trindade, S., De Niz, M. & Figueiredo, L. M. Tissue tropism in parasitic diseases. *Open Biol.* **9**, (2019).

72. Florencio-Martínez, L., Márquez-Dueñas, C., Ballesteros-Rodea, G., Martínez-Calvillo, S. & Manning-Cela, R. Cellular analysis of host cell infection by different developmental stages of Trypanosoma cruzi. *Exp. Parasitol.* **126**, 332–336 (2010).

73. Oliver, M. H., Harrison, N. K., Bishop, J. E., Cole, P. J. & Laurent, G. J. A rapid and convenient assay for counting cells cultured in microwell plates: application for assessment of growth factors. *J. Cell Sci.* **92 (Pt 3)**, 513–518 (1989).

74. Felice, D. L., Sun, J. & Liu, R. H. A modified methylene blue assay for accurate cell counting. *J. Funct. Foods* **1**, 109–118 (2009).

75. Lee, H. Z., Leung, H. W. C., Lai, M. Y. & Wu, C. H. Baicalein Induced Cell Cycle Arrest and Apoptosis in Human Lung Squamous Carcinoma CH27 Cells. *ANTICANCER Res.* 6 (2005).

76. Wang, C.-Z., Li, X.-L., Wang, Q.-F., Mehendale, S. R. & Yuan, C.-S. Selective fraction of Scutellaria baicalensis and its chemopreventive effects on MCF-7 human breast cancer cells. *Phytomedicine Int. J. Phytother. Phytopharm.* **17**, 63–68 (2010).

77. Haddad, A. Q. *et al.* Novel antiproliferative flavonoids induce cell cycle arrest in human prostate cancer cell lines. *Prostate Cancer Prostatic Dis.* **9**, 68–76 (2006).

78. Yokoi, A. *et al.* Profiling Novel Sulfonamide Antitumor Agents with Cell-based Phenotypic Screens and Array-based Gene Expression Analysis. *Mol. Cancer Ther.* **1**, 275–286 (2002).

79. Owa, T. *et al.* Discovery of Novel Antitumor Sulfonamides Targeting G1 Phase of the Cell Cycle. *J. Med. Chem.* **42**, 3789–3799 (1999).

80. Teixeira, S. A. *et al.* The Carbonic Anhydrase Inhibitor E7070 Sensitizes Glioblastoma Cells to Radio- and Chemotherapy and Reduces Tumor Growth. *Mol. Neurobiol.* **58**, 4520–4534 (2021).

81. Ferreira, D., Cortez, M., Atayde, V. D. & Yoshida, N. Actin Cytoskeleton-Dependent and -Independent Host Cell Invasion by Trypanosoma cruzi Is Mediated by Distinct Parasite Surface Molecules. *Infect. Immun.* **74**, 5522–5528 (2006).

Appendix

1. Supplementary images

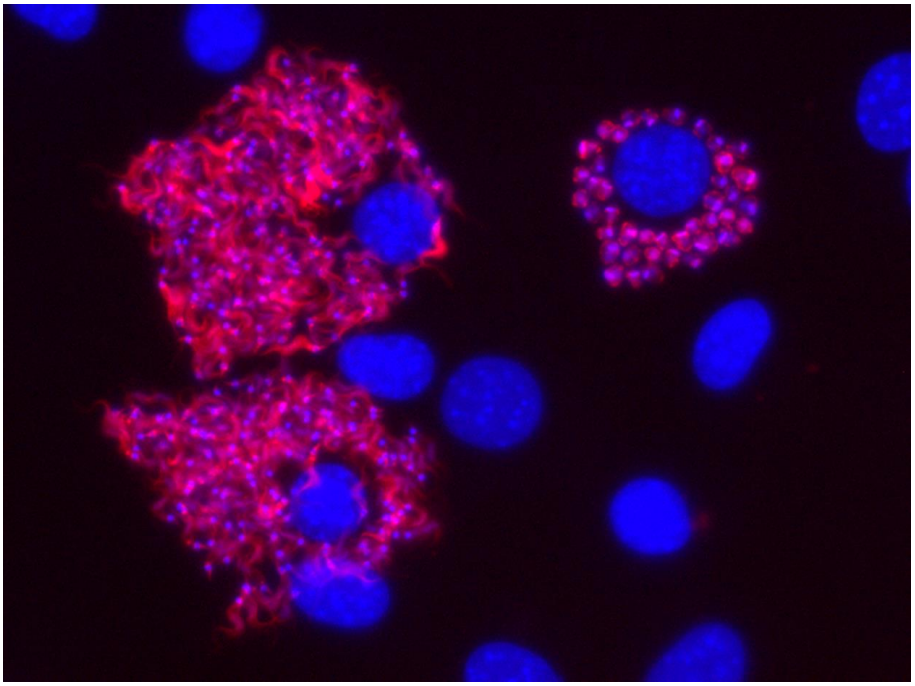

Figure S.1.: 3T3-NIH cells 96h after infection. Two of the infected cells are in direct contact full of trypomastigotes, in a very advanced state of infection. The other infected cell has a great number of amastigotes. Red: parasites (RFP), blue: nucleus (DAPI). Epifluorescence microscope (40x)

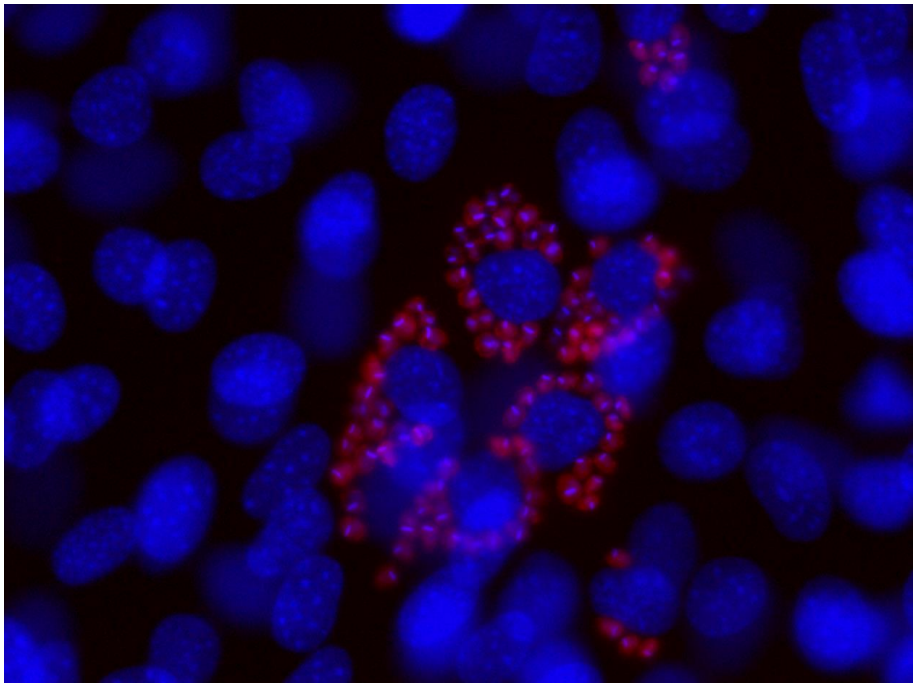

Figure S.2.: 3T3-NIH cells 96h after infection. There is cluster of 6-7 infected cells. Red: parasites (RFP), blue: nucleus (DAPI). Epifluorescence microscope (40x)

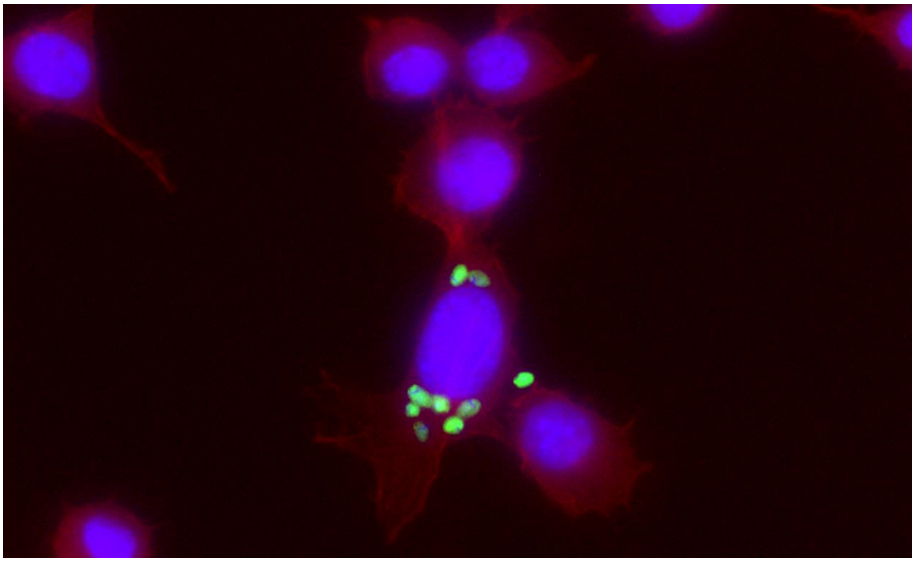

Figure S.3.: 3T3-S cells 48h after infection. Two cells are in direct contact, one of them infected. In the middle of the two cells, there is a connection area rich in actin in which a parasite could be passing from one cell to the other. Green: parasites (GFP); red: filamentous actin (phalloidin rhodamine), blue: nucleus (DAPI). Epifluorescence microscope (40x)

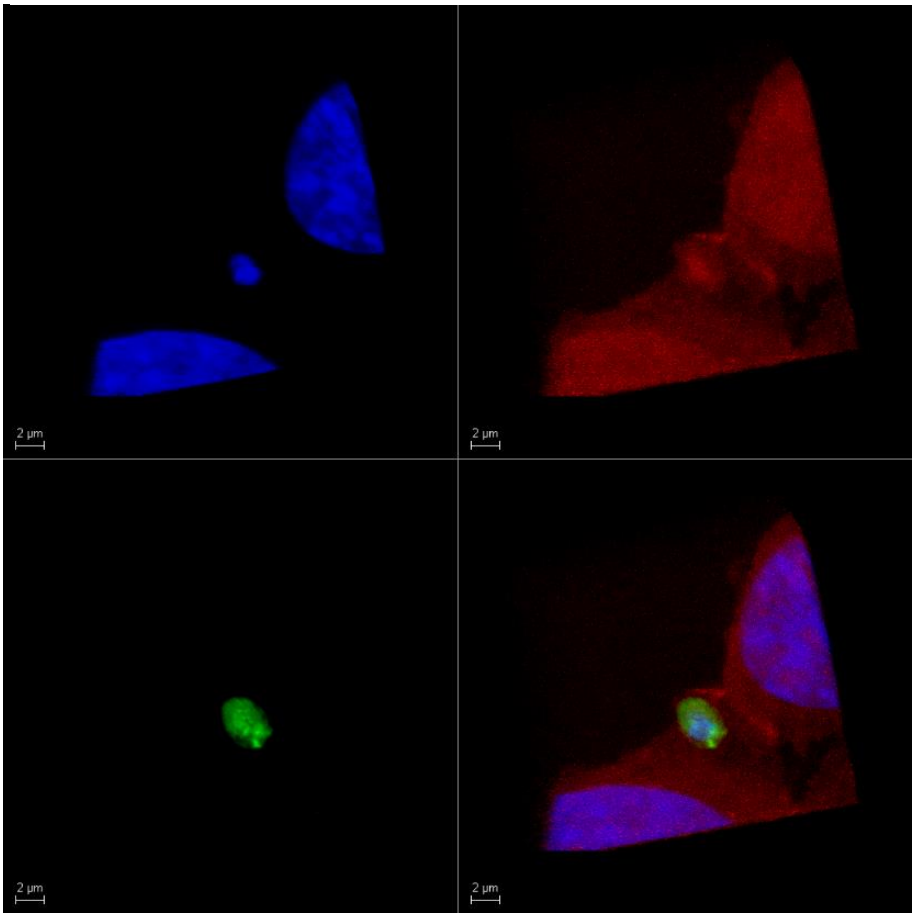

Figure S.4.: Parasite potentially being transferred cell-to-cell observed by confocal microscopy. From top-left to right-bottom: nucleus, actin cytoskeleton, parasite, and merged. An actin enriched region can be observed at the parasite location.